Extraction of $B_s \to D_s^{(*)}$ form factors from $N_f = 2$ lattice QCD

Benoit Blossier[1], Pierre-Henri Cahue[2], Jochen Heitger[3], Simone La Cesa[1],
Jan Neuendorf[1,3], and Savvas Zafeiropoulos[4]

[1]*Laboratoire de Physique des 2 Infinis Irène Joliot-Curie, CNRS/IN2P3, Université Paris-Saclay,
Bâtiment 210, 91405 Orsay Cedex, France*
[2]*Laboratoire de Physique Subatomique et de Cosmologie (LPSC), Université Grenoble-Alpes,
CNRS/IN2P3, 53 Avenue des Martyrs, F-38026 Grenoble, France*
[3]*Institut für Theoretische Physik, Westfälische Wilhelms-Universität Münster,
Wilhelm-Klemm-Street 9, 48149 Münster, Germany*
[4]*Aix Marseille Université, Université de Toulon, CNRS, CPT, Marseille, France*

We report on a two-flavor lattice QCD study of the $B_s \to D_s$ and $B_s \to D_s^*$ transitions parametrized, in the heavy quark limit, by the form factors $\mathcal{G}$, and h_{A_1}, h_{A_2}, and h_{A_3}, respectively. In the search for New Physics through tests of lepton flavor universality, B_s decay channels are complementary to the B decays widely studied at B factories and LHCb, while on the theory side they can be better controlled than the B_c and Λ_b decays. The purpose of this exploratory two-flavor study is, in preparation for future analyses of lattice QCD simulations with $N_f > 2$ and physical quark masses, to gain experience on a suitable method for a lattice extraction of form factors associated with $b \to c$ currents that may yield tighter control over systematic effects like contamination from excited states and cutoff effects. We obtain the zero-recoil values $\mathcal{G}^{B_s \to D_s}(1) = 1.03(14)$ and $h^{B_s \to D_s^*}(1) = 0.85(16)$.

I. INTRODUCTION

Although the Standard Model of particle physics (SM) has shown to describe the fundamental interactions up to the electroweak scale pretty well, experimental measurements sometimes give results that were totally unexpected. In particular, a recent and spectacular example in flavor physics phenomenology is the so-called B anomalies in the test of lepton flavor universality in $b \to c$ semileptonic decays. The ratio of decay widths $R_{H_c} \equiv \frac{\Gamma(H_b \to H_c \tau \nu_\tau)}{\Gamma(H_b \to H_c \ell \nu_\ell)_{\ell = e, \mu}}$ has been considered in cases $(H_b, H_c) = (B, D)$, (B, D^*), and $(B_c, J/\psi)$ and compared with theoretical expectations. A discrepancy of 2σ has been observed for R_D [1–10], 3σ for R_{D^*} [8–15], and $\sim\sigma$ for $R_{J/\psi}$ [16,17]. A bunch of New Physics models have been advocated to explain those discrepancies, together with other anomalies in $b \to s \ell \ell$ transitions, like models with extra doublets of Higgs fields [18] or with leptoquarks [19]. Further measurements are led to explore more $b \to c$ processes, such as $\Lambda_b \to \Lambda_c l \nu_l$ or $B_s \to D_s^{(*)} l \nu$, and are expected to come soon at LHCb and Belle 2.

A theoretical effort has been undertaken to extract the form factors associated with $B_s \to D_s^{(*)} l \nu$, but the number of results is still limited [20–25]. Our aim here is to study whether Wilson-Clover fermions, in combination with the step scaling in mass method [20,26], provide a suitable lattice regularization to get reliable results for these processes, as far as cutoff effects and contamination by excited states are concerned. While our current exploratory work focuses on $N_f = 2$, any phenomenologically relevant application of the methods investigated here has to be done in lattice QCD with $N_f = 2 + 1(+1)$ flavors.

The paper is organized as follows. In Sec. II, we highlight the strategy we have come up with. In Sec. III, we give the simulation details and collect our raw data. In Sec. IV, we present our analysis and comment on the results. Section V contains the conclusion.

II. STRATEGY

The starting point is to consider the hadronic matrix element $\langle D_s(p_{D_s}) | V^\mu | H_s(p_{H_s}) \rangle$, with $V^\mu = \bar{c} \gamma^\mu h$. Its Lorentz structure decomposition reads

$$\langle D_s(p_{D_s}) | V^\mu | H_s(p_{H_s}) \rangle = f^+(q^2)(p_{D_s} + p_{H_s})^\mu + f^-(q^2) q^\mu,$$

$$\text{(2.1)}$$

with the quantities f^+ and f^- familiar as form factors depending on $q = p_{H_s} - p_{D_s}$. We are interested in the physics case $H_s \equiv B_s$. In phenomenology, it is convenient to introduce the scalar form factor f_0 defined by

$$\langle D_s(p_{D_s})|V^\mu|H_s(p_{H_s})\rangle$$
$$= f^+(q^2)\left[(p_{D_s} + p_{H_s})^\mu - \frac{m_{H_s}^2 - m_{D_s}^2}{q^2}q^\mu\right]$$
$$+ f_0(q^2)\frac{m_{H_s}^2 - m_{D_s}^2}{q^2}q^\mu, \quad (2.2)$$

Hence, we have

$$f^-(q^2) = \frac{m_{H_s}^2 - m_{D_s}^2}{q^2}[f_0(q^2) - f^+(q^2)], \quad (2.3)$$

$$f_0(q^2) = f^+(q^2) + f^-(q^2)\frac{q^2}{m_{H_s}^2 - m_{D_s}^2}. \quad (2.4)$$

With the kinematical configuration of an H_s meson at rest, we can write

$$\langle D_s(p_{D_s})|V^0|H_s(p_{H_s})\rangle = f^+(q^2)(E_{D_s} + m_{H_s})$$
$$+ f^-(q^2)(m_{H_s} - E_{D_s}),$$
$$\langle D_s(p_{D_s})|V^i|H_s(p_{H_s})\rangle = -q^i(f^+(q^2) - f^-(q^2)). \quad (2.5)$$

When the H_s meson is put at rest, the recoil $w = \frac{p_{D_s}\cdot p_{H_s}}{m_{H_s}m_{D_s}} \equiv v_{H_s} \cdot v_{D_s}$ has the simple expression $w = E_{D_s}/m_{D_s}$. Our goal is to extract the form factor $f^+(B_s \to D_s)$ at zero recoil, $w = 1$. However, except in the elastic case $D_s \to D_s$ where one finds trivially that $f^+(w = 1) = 1$, this kinematical point is not directly accessible to a lattice measurement. It is only by extrapolating in w that one can obtain results at zero recoil. With $\vec{q} = -(\theta, \theta, \theta)$, $w \sim \sqrt{m_{D_s}^2 + 3\theta^2}/m_{D_s}$, we have

$$f^+(w) = \frac{1}{2m_{H_s}}\left[\langle D_s(p_{D_s})|V^0|H_s(p_{H_s})\rangle\right.$$
$$\left. + \frac{m_{H_s} - E_{D_s}}{3\theta}\sum_i \langle D_s(p_{D_s})|V^i|H_s(p_{H_s})\rangle\right],$$

$$f^-(w) = \frac{1}{2m_{H_s}}\left[\langle D_s(p_{D_s})|V^0|H_s(p_{H_s})\rangle\right.$$
$$\left. - \frac{m_{H_s} + E_{D_s}}{3\theta}\sum_i \langle D_s(p_{D_s})|V^i|H_s(p_{H_s})\rangle\right]. \quad (2.6)$$

On the other hand, in the framework of heavy quark effective theory (HQET), it is also common to parametrize the matrix element in question in terms of the form factors $h^\pm(w)$,

$$\frac{\langle D_s(p_{D_s})|V^\mu|H_s(p_{H_s})\rangle}{\sqrt{m_{D_s}m_{H_s}}} = h^+(w)(v_{D_s} + v_{H_s})^\mu$$
$$+ h^-(w)(v_{H_s} - v_{D_s})^\mu, \quad (2.7)$$

$$h^+(w) = \frac{1}{2\sqrt{m_{D_s}m_{H_s}}}[(m_{H_s} + m_{D_s})f^+(w)$$
$$+ (m_{H_s} - m_{D_s})f^-(w)],$$

$$h^-(w) = \frac{1}{2\sqrt{m_{D_s}m_{H_s}}}[(m_{H_s} - m_{D_s})f^+(w)$$
$$+ (m_{H_s} + m_{D_s})f^-(w)], \quad (2.8)$$

with the aid of which one introduces the factors $\mathcal{G}(w)$ and $H(w)$,

$$\mathcal{G}(w) = h^+(w)\left[1 - \frac{m_{H_s} - m_{D_s}}{m_{H_s} + m_{D_s}}\frac{h^-(w)}{h^+(w)}\right]$$
$$= h^+(w)\left[1 - \left(\frac{m_{H_s} - m_{D_s}}{m_{H_s} + m_{D_s}}\right)^2 H(w)\right], \quad (2.9)$$

$$H(w) = \frac{m_{H_s} + m_{D_s}}{m_{H_s} - m_{D_s}}\frac{h^-(w)}{h^+(w)}. \quad (2.10)$$

$h^\pm(1)$, $f^\pm(1)$, and $f_0(1)$ can then be extracted by doing a polynomial extrapolation in $w - 1$. In the following, we concentrate on estimating of $\mathcal{G}^{B_s \to D_s}(w = 1)$.

To obtain results at the b quark mass (while trying to keep cutoff effects under control), we have decided to apply the strategy of step scaling in masses [20,26] that was already adapted to the Wilson-Clover regularization in [27]. Steps in renormalization group invariant (RGI) heavy quark mass cannot be used at this stage of knowledge as far as the Wilson-Clover regularization is concerned. Indeed, without a still unknown $O(a^2)$ term in an improvement factor, the RGI quark mass becomes negative, hence unphysical, for quark masses greater than $\sim 2m_c$ and the lattice spacings at our disposal.

The idea is to consider ratios of $\mathcal{G}(1)$ at two consecutive heavy-strange meson masses $m_{H_s(i+1)}$ and $m_{H_s(i)}$ in the step-scaling mass chain,

$$\sigma_\mathcal{G}^i = \frac{\mathcal{G}(1, m_{H_s(i+1)})}{\mathcal{G}(1, m_{H_s(i)})}, \quad m_{H_s(i)} = \lambda^i m_{D_s}, \quad \lambda = \left(\frac{m_{B_s}}{m_{D_s}}\right)^{1/K}, \quad (2.11)$$

where K is the number of steps. Thus, we have

$$\mathcal{G}(1, m_{B_s}) = \mathcal{G}(1, m_{D_s}) \times \prod_{i=0}^{K-1} \sigma_\mathcal{G}^i, \quad (2.12)$$

with

$$\mathcal{G}(1, m_{D_s}) = \lim_{a \to 0, m_\pi \to m_\pi^{\text{phys}}} \mathcal{G}^{\text{lat}}(1, m_{D_s}, a, m_\pi), \quad (2.13)$$

$$\sigma_{\mathcal{G}}^i = \lim_{a \to 0, m_\pi \to m_\pi^{\text{phys}}} \Sigma_{\mathcal{G}}^i(a, m_\pi), \quad (2.14)$$

where $\Sigma_{\mathcal{G}}^i = \frac{\mathcal{G}^{\text{lat}}(m_{H_s(i)})}{\mathcal{G}^{\text{lat}}(m_{H_s(i-1)})}$ is the ratio of successive $\mathcal{G}$'s on the given ensemble. By construction, $\mathcal{G}(1, m_{D_s})$ is equal to 1. It is a useful check that our numerical data obey that constraint. Taking this into account, we have $\mathcal{G}(1, m_{B_s}) = \prod_{i=0}^{K-1} \sigma_{\mathcal{G}}^i$.

Concerning the decay $H_s \to D_s^*$, a convenient framework is again HQET. Taking into account parities under C, P, and T symmetries, the Lorentz structure decomposition of the hadronic matrix element $\langle D_s^*(p_{D_s^*}, \epsilon^{(\lambda)}) | A^\mu | H_s(p_{H_s}) \rangle$ reads

$$\frac{\langle D_s^*(p_{D_s^*}, \epsilon^{(\lambda)}) | A^\mu | H_s(p_{H_s}) \rangle}{2\sqrt{m_{H_s} m_{D_s^*}}} = \frac{i}{2} \epsilon_\nu^{*(\lambda)} [g^{\mu\nu}(1 + w)h_{A_1}$$
$$- v_{H_s}^\mu (v_{B_s}^\nu h_{A_2} + v_{D_s^*}^\nu h_{A_3})]. \quad (2.15)$$

With

$$R^{\mu\rho} = \sum_\lambda \epsilon^{\rho(\lambda)} \langle D_s^*(p_{D_s^*}, \epsilon^{(\lambda)}) | A^\mu | H_s(p_{H_s}) \rangle, \quad (2.16)$$

and the normalization equation of the polarization vectors of a vector meson of mass m_V and momentum k,

$$\sum_\lambda \epsilon^{\mu(\lambda)} \epsilon^{*\nu(\lambda)} = -g^{\mu\nu} + \frac{k^\mu k^\nu}{m_V^2}, \quad (2.17)$$

we get

$$\frac{-R^{\mu\rho}}{2\sqrt{m_{H_s} m_{D_s^*}}}$$
$$= \frac{i}{2} \left[\left(g^{\mu\rho} - \frac{p_{D_s^*}^\mu p_{D_s^*}^\rho}{m_{D_s^*}^2} \right)(1 + w)h_{A_1} \right.$$
$$\left. - \left(g^{\rho\nu} - \frac{p_{D_s^*}^\rho p_{D_s^*}^\nu}{m_{D_s^*}^2} \right)(v_{\nu B_s} v_{H_s}^\mu h_{A_2} + v_{\nu B_s} v_{D_s^*}^\mu h_{A_3}) \right]. \quad (2.18)$$

Taking the H_s meson at rest and i, j as spatial indices, we obtain

$$\frac{-R^{ij}}{2\sqrt{m_{H_s} m_{D_s^*}}} = \frac{i}{2} \left[\left(g^{ij} - \frac{p_{D_s^*}^i p_{D_s^*}^j}{m_{D_s^*}^2} \right)(1 + w)h_{A_1} \right.$$
$$\left. + \frac{E_{D_s^*} p_{D_s^*}^i p_{D_s^*}^j}{m_{D_s^*}^3} h_{A_3} \right]. \quad (2.19)$$

It means that we can determine two form factors, h_{A_1} and h_{A_3}. With

$$A = \frac{1}{2\sqrt{m_{H_s} m_{D_s^*}}} \frac{i}{3} \sum_i R^{ii},$$

$$B = \frac{1}{2\sqrt{m_{H_s} m_{D_s^*}}} \frac{i}{6} \sum_{i \neq j} R^{ij}, \quad (2.20)$$

and an isotropic momentum $\vec{p}_{D_s^*} = (\theta, \theta, \theta)$, we have

$$A = \frac{1}{2} \left[\left(1 + \frac{\theta^2}{m_{D_s^*}^2} \right)(1 + w)h_{A_1} - \frac{E_{D_s^*} \theta^2}{m_{D_s^*}^3} h_{A_3} \right],$$

$$B = \frac{1}{2} \left(\frac{\theta^2}{m_{D_s^*}^2} (1 + w)h_{A_1} - \frac{E_{D_s^*} \theta^2}{m_{D_s^*}^3} h_{A_3} \right). \quad (2.21)$$

Thus, we arrive at

$$h_{A_1} = \frac{2}{w + 1}(A - B), \quad (2.22)$$

$$h_{A_3} = \frac{m_{D_s^*}^3}{E_{D_s^*} \theta^2} \left[(w + 1) \frac{\theta^2}{m_{D_s^*}^2} h_{A_1} - 2B \right]. \quad (2.23)$$

According to our step-scaling procedure, these quantities can finally be expressed as

$$h_{A_1}(1, m_{B_s}) = h_{A_1}(1, m_{D_s}) \times \prod_{i=0}^{K-1} \sigma_{h_{A_1}}^i \quad (2.24)$$

$$R_{X_3}(1, m_{B_s}) \equiv \frac{h_{A_3}(1, m_{B_s})}{h_{A_1}(1, m_{B_s})}$$
$$= R_{X_3}(1, m_{D_s}) \times \prod_{i=0}^{K-1} \sigma_{R_{X_3}}^i, \quad (2.25)$$

with

$$h_{A_1}(1, m_{D_s}) = \lim_{a \to 0, m_\pi \to m_\pi^{\text{phys}}} h_{A_1}^{\text{lat}}(1, m_{D_s}, a, m_\pi), \quad (2.26)$$

$$\sigma_Y^i = \lim_{a \to 0, m_\pi \to m_\pi^{\text{phys}}} \Sigma_Y^i(a, m_\pi), \quad Y = h_{A_1}, R_{X_3}. \quad (2.27)$$

III. COMPUTATIONAL SETUP

We have used in our analysis gauge field configuration ensembles generated by the CLS (Coordinated Lattice Simulations) effort with $N_f = 2$ nonperturbatively $O(a)$ improved Wilson-Clover fermions [28,29] and the plaquette gauge action [30]. The parameter κ_s was taken from [31] and κ_c from [32]. They have been used in previous works, e.g., [27,33].

We have injected momenta to quarks by imposing isotropic twisted-boundary conditions in space, i.e., $\psi(x + L\vec{e}_i) = e^{i\theta_i}\psi(x)$ with twisting angles θ_i, $i = 1, 2, 3$. The kinematics for two-point and three-point correlation

TABLE I.   Parameters of the simulations: bare coupling $\beta = 6/g_0^2$, lattice resolution, hopping parameters of strange- and charm-quark masses, lattice spacing a in physical units, pion mass, number of gauge configurations, and bare strange and charm quark masses. (Ensembles with * were excluded from the extraction of h_{A_1}).

Id	β	$\left(\frac{L}{a}\right)^3 \times \frac{T}{a}$	κ_{sea}	a (fm)	$\frac{m_\pi}{\text{MeV}}$	Lm_π	Number of configurations	κ_s	κ_c
A5	5.2	$32^3 \times 64$	0.13594	0.0751	333	4.1	198	0.135267	0.12531
B6*		$48^3 \times 96$	0.13597		282	5.2	118	0.135257	0.12529
E5	5.3	$32^3 \times 64$	0.13625	0.0653	439	4.7	200	0.135777	0.12724
F6		$48^3 \times 96$	0.13635		313	5	120	0.135741	0.12713
F7		$48^3 \times 96$	0.13638		268	4.3	200	0.135730	0.12713
G8*		$64^3 \times 128$	0.13642		194	4.1	100	0.135705	0.12710
N6	5.5	$48^3 \times 96$	0.13667	0.0483	341	4	192	0.136250	0.13026
O7		$64^3 \times 128$	0.13671		269	4.2	60	0.136243	0.13022

functions are depicted in Fig. 1, where strange, charm, and heavy flavors are denoted by s, c, and h, respectively. Only the charm quark carries the nonzero momentum. To reduce some of the $O(a^2)$ effects, we have averaged our results over positive and negative momenta. Six pairs $\pm\vec{\theta}$, in addition to the zero-momentum point, help us to extrapolate the various form factors associated with $H_s \rightarrow D_s$ and $H_s \rightarrow D_s^*$ from data available in the recoil region $1 \leq w \lesssim 1.1$.

In Table I, we collect the parameter specifications of the ensembles. Three lattice spacings $a_{\beta=5.5} = 0.04831(38)$ fm, $a_{\beta=5.3} = 0.06531(60)$ fm, $a_{\beta=5.2} = 0.07513(79)$ fm, where the scale setting was performed in [34] via a fit in the chiral sector, are considered with pion masses in the range [190 MeV, 440 MeV]. Heavy bare quark masses are the same as in [27]. Statistical errors have been computed employing the "Γ-method" [35], based on estimating autocorrelation functions.[1] As in [27], all-to-all propagators were estimated stochastically with $U(1)$ spin-diluted wall-time noise sources. We have also reduced the contamination by excited states on two-point and three-point correlators by solving a 4×4 generalized eigenvalue problem (GEVP) with one local and three Gaussian smeared interpolating fields. In the mass step-scaling strategy outlined above, we set $K = 6$. In Table II, we collect the twisting angles used to inject momenta to the charm quark. The phase shift was applied isotropically in all spatial directions.

Our analysis involves the following two-point correlation functions evaluated on the gauge field ensembles at hand,

$$C_{ij}^{\theta,D_s}(t) = \sum_{\vec{x}}\langle P_{cs,i}^{\theta}(t)P_{cs,j}^{\dagger\theta}(0)\rangle,$$

$$C_{ij}^{H_s}(t) = \sum_{\vec{x}}\langle P_{hs,i}(t)P_{hs,j}^{\dagger}(0)\rangle,$$

$$C_{ij}^{\theta,D_s^*}(t) = \frac{1}{3}\sum_{k=1}^{3}\sum_{\vec{x}}\langle V_{cs,k,i}^{\theta}(t)V_{cs,k,j}^{\dagger\theta}(0)\rangle, \quad (3.1)$$

where quark labels are as above, i and j specify smearing labels, and spatial coordinates (summed over) are suppressed. The entering quark bilinears are defined as $P_{hs} = \bar{\psi}_h\gamma^5\psi_s$, $P_{cs}^{\theta} = \bar{\psi}_c^{\theta}\gamma^5\psi_s$, and $V_{cs,k}^{\theta} = \bar{\psi}_c^{\theta}\gamma_k\psi_s$.

Now, we continue with the three-point correlation functions,

$$C_{ij}^{\theta,PV_\mu^I P}(t_i,t) = \sum_{\vec{x},\vec{y}}\langle P_{hs,i}(t_i)V_{hc,\mu}^{I,\theta}(t)P_{cs,j}^{\dagger\theta}(0)\rangle,$$

$$C_{ij}^{\theta,PA_k^I V_l}(t_i,t) = \sum_{\vec{x},\vec{y}}\langle P_{hs,i}(t_i)A_{hc,\mu}^{I,\theta}(t)V_{cs,l,j}^{\dagger\theta}(0)\rangle, \quad (3.2)$$

where the improved currents read $V_{hc,\mu}^{I,\theta} = \bar{\psi}_h\gamma_\mu\psi_c^{\theta} + ac_V\tilde{\partial}_\nu(\bar{\psi}_h\sigma_{\mu\nu}\psi_c^{\theta})$ and $A_{hc}^{I,\theta} = \bar{\psi}_c^{\theta}\gamma_k\gamma^5\psi_h + ac_A\tilde{\partial}_k(\bar{\psi}_c^{\theta}\gamma^5\psi_h)$ with $\tilde{\partial}_\mu f(x) \equiv \frac{1}{2}(f(x+a\hat{\mu}) - f(x-a\hat{\mu}))$.

Accordingly, we have to solve the three GEVPs,

$$C_{ij}^{\theta,D_s}(t)v_j^{\theta,D_s}(t,t_0) = \lambda^{\theta,D_s}(t,t_0)C_{ij}^{\theta,D_s}(t_0)v_j^{\theta,D_s}(t,t_0),$$

$$C_{ij}^{H_s}(t)v_j^{H_s}(t,t_0) = \lambda^{H_s}(t,t_0)C^{H_s}(t_0)_{ij}v_j^{H_s}(t,t_0),$$

$$C_{ij}^{\theta,D_s^*}(t)v_j^{\theta,D_s^*}(t,t_0) = \lambda^{\theta,D_s^*}(t,t_0)C_{ij}^{\theta,D_s^*}(t_0)v_j^{\theta,D_s^*}(t,t_0). \quad (3.3)$$

Then, we project the two-point and three-point correlation functions onto the generalized eigenvector chosen at a given time t_{fix}, $\vec{b} \equiv \vec{v}(t_{\text{fix}},t_0)$,
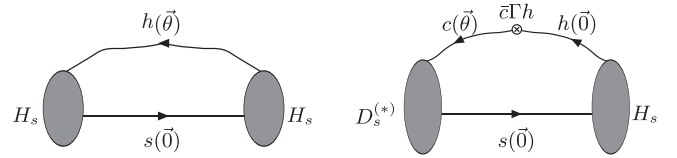

FIG. 1.   Kinematical configuration of the two-point and three-point correlation functions under study to extract the $H_s \rightarrow D_s^{(*)}$ form factors: the strange quark is always set at rest, while the $h \rightarrow c$ current inherits its momentum from the charm quark boundary condition. Γ specifies the Dirac structure in question.

TABLE II. Twisted angles of the charm quark field boundary condition that we use to inject momenta at the $h \to c$ current.

Id	$\theta[\pi/L]$
A5	$\{0.000, \pm0.150, \pm0.300, \pm0.525, \pm0.750, \pm1.050, \pm1.275\}$
B6	$\{0.000, \pm0.163, \pm0.326, \pm0.571, \pm0.815, \pm1.141, \pm1.385\}$
E5	$\{0.000, \pm0.125, \pm0.250, \pm0.438, \pm0.625, \pm0.875, \pm1.062\}$
F6	$\{0.000, \pm0.188, \pm0.375, \pm0.656, \pm0.938, \pm1.312, \pm1.594\}$
F7	$\{0.000, \pm0.188, \pm0.375, \pm0.656, \pm0.938, \pm1.312, \pm1.594\}$
G8	$\{0.000, \pm0.250, \pm0.500, \pm0.875, \pm1.250, \pm1.750, \pm2.125\}$
N6	$\{0.000, \pm0.254, \pm0.507, \pm0.887, \pm1.262, \pm1.774, \pm2.155\}$
O7	$\{0.000, \pm0.338, \pm0.676, \pm1.183, \pm1.683, \pm2.365, \pm2.873\}$

$$\tilde{C}^{\theta,D_s}(t) \equiv b_i^{\theta,D_s} C_{ij}^{\theta,D_s}(t) b_j^{\theta,D_s},$$
$$\tilde{C}^{H_s}(t) \equiv b_i^{H_s} C_{ij}^{H_s}(t) b_j^{H_s},$$
$$\tilde{C}^{\theta,D_s^*}(t) \equiv b_i^{\theta,D_s^*} C_{ij}^{\theta,D_s^*}(t) b_j^{\theta,D_s^*},$$
$$\tilde{C}^{\theta,PV_\mu^I P}(t_i,t) \equiv b_i^{H_s} C_{ij}^{\theta,PV_\mu^I P}(t_i,t) b_j^{\theta,D_s},$$
$$\tilde{C}^{\theta,PA_k^I V_l}(t_i,t) \equiv b_i^{H_s} C_{ij}^{\theta,PA_k^I V_l}(t_i,t) b_j^{\theta,D_s^*}. \tag{3.4}$$

The asymptotic behavior of the two-point functions is known to be given by

$$\tilde{C}^{\theta,D_s}(t) \xrightarrow{t/a \gg 1} \frac{\mathcal{Z}^{\theta,D_s}}{2E_{D_s}} \exp^{-E_{D_s}T/2} \cosh\left[E_{D_s}\left(t-\frac{T}{2}\right)\right],$$

$$\tilde{C}^{H_s}(t) \xrightarrow{t/a \gg 1} \frac{\mathcal{Z}^{H_s}}{2m_{H_s}} \exp^{-m_{H_s}T/2} \cosh\left[m_{H_s}\left(t-\frac{T}{2}\right)\right],$$

$$\tilde{C}^{\theta,D_s^*}(t) \xrightarrow{t/a \gg 1} \frac{\mathcal{Z}^{\theta,D_s^*}}{2E_{D_s^*}}\left(1+\frac{\theta^2}{m_{D_s^*}}\right)\exp^{-E_{D_s^*}T/2}$$
$$\times \cosh\left[E_{D_s^*}\left(t-\frac{T}{2}\right)\right]. \tag{3.5}$$

Finally, the desired matrix elements may be computed from the large-time asymptotics of suitable ratios of the foregoing two-point and three-point correlation functions as

$$\frac{\tilde{C}^{\theta,PV_\mu^I P}(t_i,t)\sqrt{\mathcal{Z}^{\theta,D_s}\mathcal{Z}^{H_s}}}{\tilde{C}^{\theta,D_s}(t)\tilde{C}^{H_s}(t_i-t)} \xrightarrow{1\ll t/a \ll (t_i-t)/a} \langle D_s(\theta)|V_\mu^I|H_s\rangle^{(b)},$$

$$\frac{\tilde{C}^{\theta,PA_k^I V_l}(t_i,t)\sqrt{\mathcal{Z}^{\theta,D_s}\mathcal{Z}^{H_s}}}{\tilde{C}^{\theta,D_s^*}(t)\tilde{C}^{H_s}(t_i-t)}\left(1+\frac{\theta^2}{m_{D_s^*}^2}\right) \xrightarrow{1\ll t/a \ll (t_i-t)/a} R_{kl}^{(b)},$$
$$\tag{3.6}$$

where the label (b) refers to bare hadronic matrix elements. Later, it is convenient to note

$$\frac{1}{3}\sum_i \langle D_s|V_i^I|H_s\rangle^{(b)} \equiv \langle D_s|\vec{V}^I|H_s\rangle^{(b)},$$

$$\frac{1}{3}\sum_i R_{ii}^{(b)} \equiv \langle D_s^*|\vec{A}^I|H_s\rangle_\parallel^{(b)}. \tag{3.7}$$

Upon mass dependent $O(a)$ improvement and multiplicative renormalization, the physical matrix elements are

$$\langle D_s(\theta)|V_\mu^I|H_s\rangle = Z_V(1+b_V am_{hc}^{VWI})\langle D_s(\theta)|V_\mu^I|H_s\rangle^{(b)},$$

$$R_{kl} = Z_A(1+b_A am_{hc}^{VWI})R_{kl}^{(b)}, \tag{3.8}$$

where the vector Ward identity mass m_{hc}^{VWI} is related to the PCAC quark masses m_{hs}^{PCAC}, m_{cs}^{PCAC}, and m_{ss}^{PCAC} by $m_{hc}^{VWI} = Z(m_{hs}^{PCAC} + m_{cs}^{PCAC} - m_{ss}^{PCAC})$. Perturbative and nonpertubative values for the coefficients Z_V, Z_A, c_V, c_A, b_V, b_A, and Z are available from [36–38].

IV. ANALYSIS

A. Extraction of hadronic matrix elements

As described in the previous section, we have solved 4×4 GEVP systems, except for the most chiral ensemble G8 for which we had to restrict the analysis to the 2×2 most smeared part of the correlators matrices, because the data are too noisy. We have set $t_0/a = 3$ and $t_{fix}/a = 6$. We vary the parameters t_{fix}, t_0, and the time ranges used to fit the two-point correlation functions and ratios of three-point and two-point correlation functions, in order to estimate the systematic errors on the hadronic matrix elements. In practice, we found that the alteration of the parameters t_0 and t_{fix} does not influence the results significantly. Moreover, we have observed that the GEVP solutions are in a large part compatible with choosing the most smeared source for our interpolating fields. These findings are illustrated in Fig. 2. The source-sink time separation t_i is equal to $T/2$.

We have obtained hadron masses am_{H_s} by fitting the plateau of the effective mass data $am^{eff}(t)$ coming from the generalized eigenvalues.[2] The fit range $[t_{min}, t_{max}]$ is chosen after a visual inspection of the plateau. The data are strongly correlated; therefore, the error of the plateau is not much smaller than the error of the individual data points. For this reason, it was more important to exclude points outside the plateau than to maximize the available statistics. The same is done to evaluate the hadronic matrix elements $\langle D_s|V_\mu^I|H_s\rangle^{(b)}$ and $R_{kl}^{(b)}$ along the formulas above.

---

[2]In practice, we got the eigenvalues by projecting the smearing matrices with the eigenvectors.
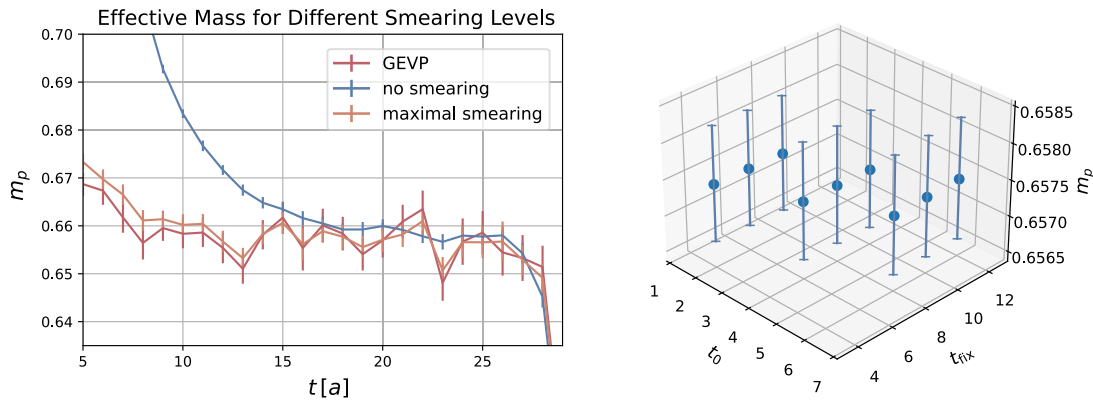
FIG. 2. Visualizations for the generalized eigenvalue problem for the D_s at rest on E5. Left: effective mass for the smearings [0,0], [80,80], and the GEVP projection. Right: result of the mass extraction with consistent plateau ranges for different GEVP parameters.

In more detail, the extraction of the matrix elements involves the following elements

(1) We apply symmetries, solve the GEVP, and project the correlators following Eq. (3.4).

(2) The masses and energies, am_{H_s} and $aE_{D_s^{(*)}}$, are extracted from a plateau of the effective mass of the projected correlator.

(3) The amplitudes $\mathcal{Z}^{\theta,H_s}$ and $\mathcal{Z}^{\theta,D_s^{(*)}}$ are obtained from a fit with Eq. (3.5).

(4) We divide the three-point correlator by $\sqrt{\frac{\mathcal{Z}^{\theta,H_s}\mathcal{Z}^{\theta,D_s^{(*)}}}{2m_{H_s}E_{D_s^{(*)}}}}e^{-E_{D_s^{(*)}}\frac{T}{2}}e^{-(m_{B_s}-E_{D_s^{(*)}})t}$ and fit the resulting plateau to get $\langle D_s(\theta)|V_\mu^I|H_s\rangle^{(b)}$ or $R_{kk}^{(b)}$ [Eq. (3.6) without the backward contributions in time].

Figures 3–6 display some effective masses of pseudoscalar and vector heavy-strange mesons and hadronic matrix elements. Raw data are collected in the Appendix.
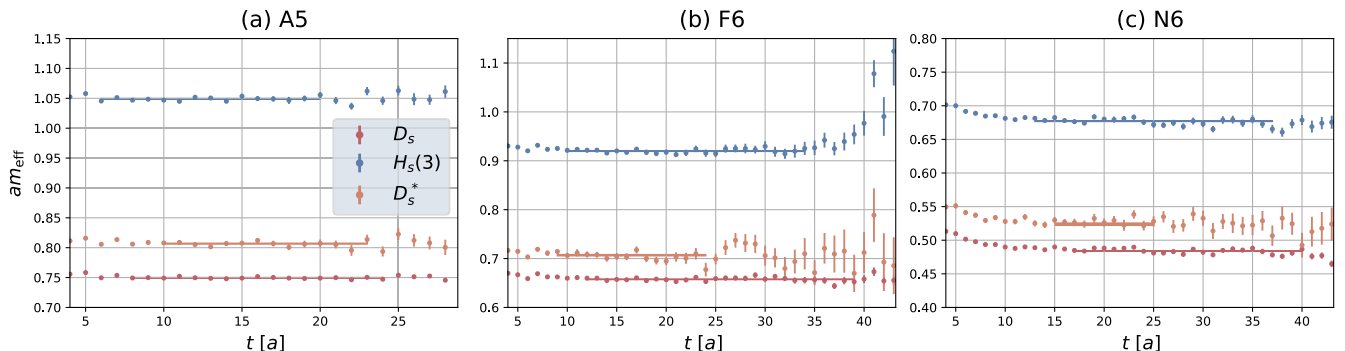
FIG. 3. Effective masses obtained from the projected two-point correlators $\tilde{C}^{0,D_s}$, $\tilde{C}^{0,D_s^*}$, and $\tilde{C}^{H_s(3)}$, together with the extracted mass. The data correspond to the ensemble A5 (a), F6 (b), and N6 (c).
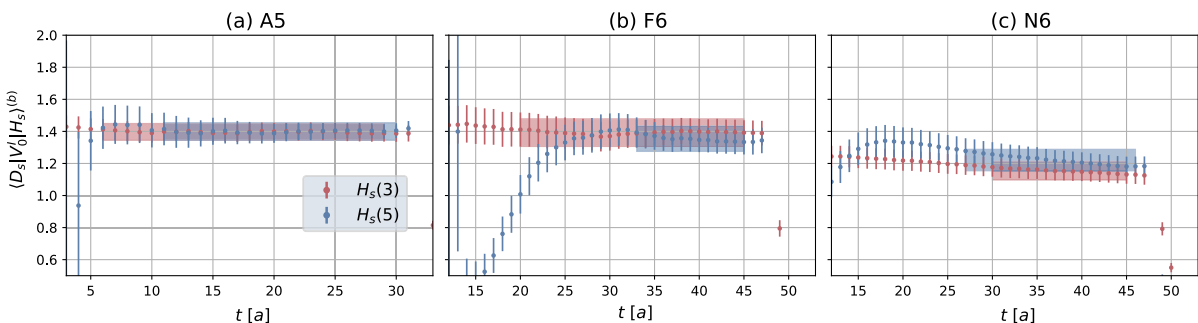
FIG. 4. Bare hadronic matrix element $\langle D_s(\theta)|V_0^I|H_s(i=\{3,5\})\rangle$ extracted from the fits according to Eq. (3.6). The data correspond to the ensemble A5, $\theta = 0.525\pi/32$ (a), F6, $\theta = 0.65625\pi/48$ (b), and N6, $\theta = 0.887\pi/48$ (c).
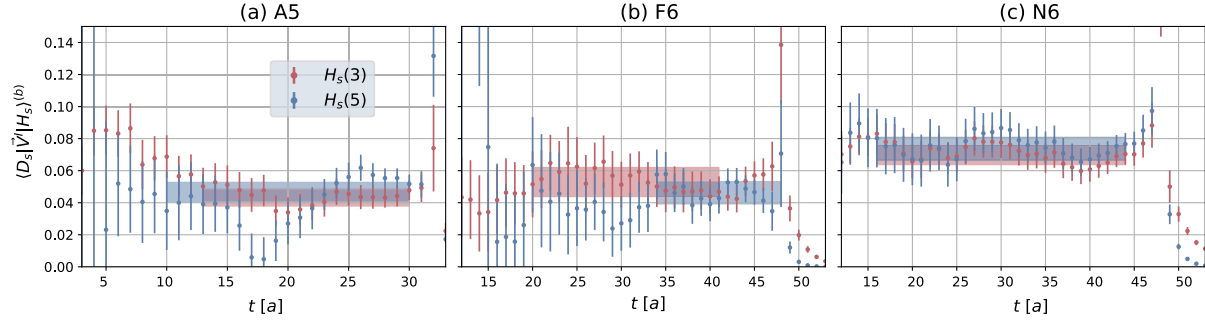
FIG. 5. Bare hadronic matrix element $\langle D_s(\theta)|\vec{V}^I|H_s(i=\{3,5\})\rangle^{(b)}$ extracted from the fits according to Eq. (3.6). The data correspond to the ensemble A5, $\theta = 0.525\pi/32$ (a), F6, $\theta = 0.65625\pi/48$ (b), and N6, $\theta = 0.887\pi/48$ (c).
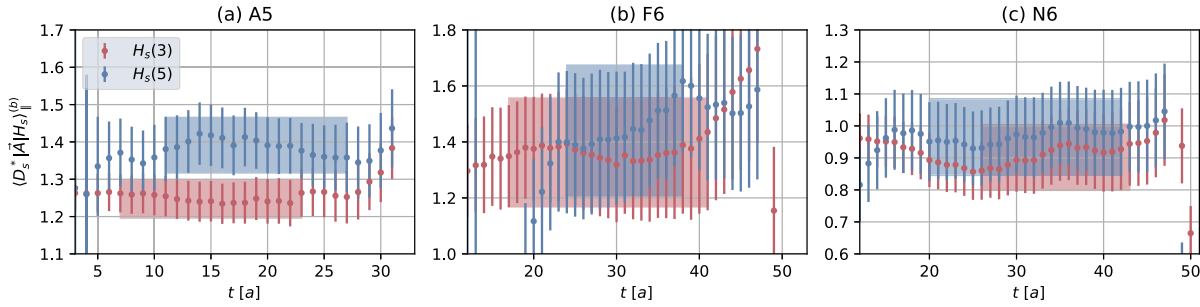
FIG. 6. Bare hadronic matrix element $\langle D_s^*(\theta)|\vec{A}|H_s(i=\{3,5\})\rangle_{\parallel}^{(b)}$ extracted from the fits according to Eq. (3.6). The data correspond to the ensemble A5, $\theta = 0.525\pi/32$ (a), F6, $\theta = 0.65625\pi/48$ (b), and N6, $\theta = 0.887\pi/48$ (c).

B. Extrapolation to the physical point

Once we have obtained the hadronic matrix elements, we are, in principle, able to determine the heavy quark symmetry form factors h^+, h^-, and $h_{A_{1,3}}$. Unfortunately, the statistical quality of our data is not sufficient to reliably calculate h_{A_3}. Therefore, we restrict ourselves to the two former quantities at nonzero recoil and on $h_{A_1}(w=1)$. We have tried to extrapolate h^+ and h^- to $w=1$ separately and compute $\mathcal{G}(1)$ from it, as well as to extrapolate $\mathcal{G}(w)$ directly. The two extrapolations are mostly compatible, because the range in w is very small. We have performed linear and quadratic extrapolations in $(w-1)$. As quadratic fit coefficients are consistent with zero for almost all ensembles, we work with the result from the linear extrapolations for the remainder of the analysis. In Fig. 7, we show extrapolations of $\mathcal{G}$ to zero recoil for a

selection of ensembles. The next-to-last step is to extrapolate $\Sigma_{\mathcal{G}}^i = \frac{\mathcal{G}(1,a,m_\pi^2,m_{H_s(i)})}{\mathcal{G}(1,a,m_\pi^2,m_{H_s(i-1)})}$ to the physical point, where i denotes the mass step-scaling step corresponding to $m_{H_s(i)} = \lambda^i m_{D_s}$. We have used the following fit ansatz:

$$\Sigma_{\mathcal{G}}^i(w=1,a,m_\pi^2) = \Sigma_{\mathcal{G},0}^i + \Sigma_{\mathcal{G},1}^i \times (a/a_{\beta=5.3})^2$$
$$+ \Sigma_{\mathcal{G},2}^i \times \left(\frac{m_\pi}{m_\pi^{\text{physical}}}\right)^2. \quad (4.1)$$

The fit parameters and $\chi^2/\text{d.o.f.}$ are collected in Table III. Two of those fits are shown in Fig. 8.

Parametrizations with additional terms were also studied. In particular, one might include a mistuning term $\left(1 - \frac{m_{H_s}}{\lambda^i m_{D_s}}\right)$ to account for the fact that the heavy meson masses are not tuned exactly equally on each ensemble.
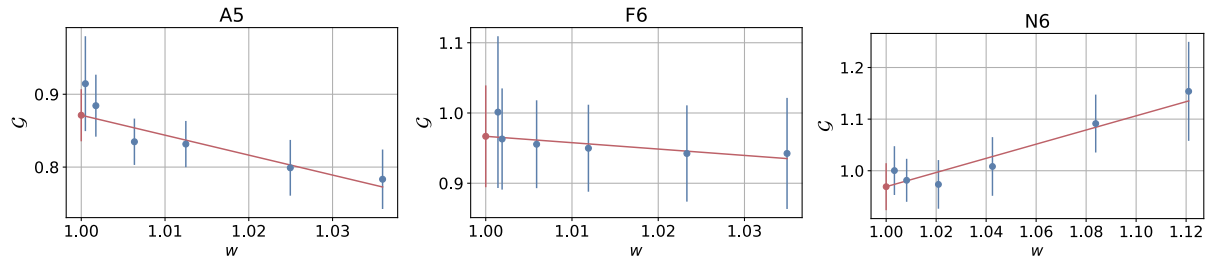
FIG. 7. Linear extrapolation of $\mathcal{G}(w)$ to the point of zero recoil ($w=1$). Examples given for three ensembles at $m_{H_s} = \lambda^2 m_{D_s}$

TABLE III. Fit parameters for the extrapolation of $\Sigma_{\mathcal{G}}^i$.

I	$\Sigma_{\mathcal{G},0}^i$	$\Sigma_{\mathcal{G},1}^i$	$\Sigma_{\mathcal{G},2}^i$	$\chi^2/\text{d.o.f.}$
1	1.018(32)	−0.033(24)	0.0006(32)	0.46924
2	1.005(25)	−0.019(18)	0.0000(27)	0.35307
3	1.011(35)	0.044(40)	−0.0057(43)	0.56284
4	0.993(33)	0.033(25)	−0.0028(29)	0.91723
5	1.007(63)	−0.010(75)	0.0009(75)	1.09348

However, we decided to only include the terms in Eq. (4.1), because the data are so noisy that the fits cannot reliably resolve these terms. In fact, as seen in Table III, only very few nonconstant terms are statistically significant. Cutoff effects are limited to 5%, while a pion mass dependence is almost absent. Then, we can write

$$\sigma_{\mathcal{G}}^i(m_\pi^{2,\text{physical}}) = \Sigma_{\mathcal{G}}^i(w=1, a=0, m_\pi^2 = m_\pi^{2,\text{physical}})$$
$$= \Sigma_{\mathcal{G}_0}^i + \Sigma_{\mathcal{G}_2}^i. \quad (4.2)$$

Unfortunately, no clear trend in m_{H_s} dependence is seen, as shown in the left panel of Fig. 9. That is why we have
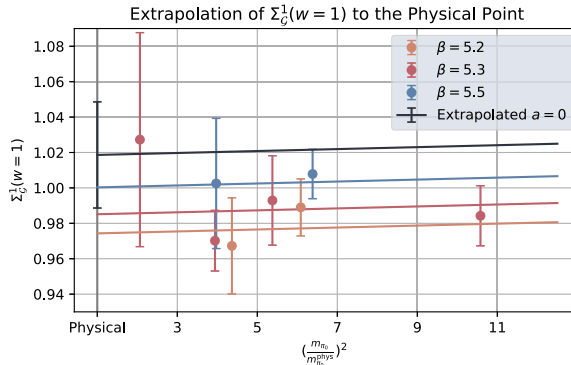
fitted the ratios $\sigma_{\mathcal{G}}^i$ by a constant $\bar{\sigma}_{\mathcal{G}}$. We get $\bar{\sigma}_{\mathcal{G}} = 1.005(23)$.

Moreover, we have checked whether our data obey the constraint $\mathcal{G}(1, m_{D_s}) = 1$. To do so, we have performed the following extrapolation:

$$\mathcal{G}(1, a, m_\pi^2, m_{D_s}) = \mathcal{G}_0 + \mathcal{G}_1 \times (m_\pi^2/m_\pi^{2,\text{physical}})$$
$$+ \mathcal{G}_2 \times (a/a_{\beta=5.3})^2. \quad (4.3)$$

The left panel of Fig. 10 shows that our continuum extrapolation $\mathcal{G}(1, m_{D_s})$ is fully compatible with 1 within the limited statistics. As a final result for $\mathcal{G}$, we quote

$$\mathcal{G}^{B_s \to D_s}(w=1) = \bar{\sigma}_{\mathcal{G}}^K = \bar{\sigma}_{\mathcal{G}}^6 = 1.03(14). \quad (4.4)$$

We have also performed a combined fit for the ratio using all data points simultaneously to explore the mass dependence and the effects of mistuning between the different ensembles,
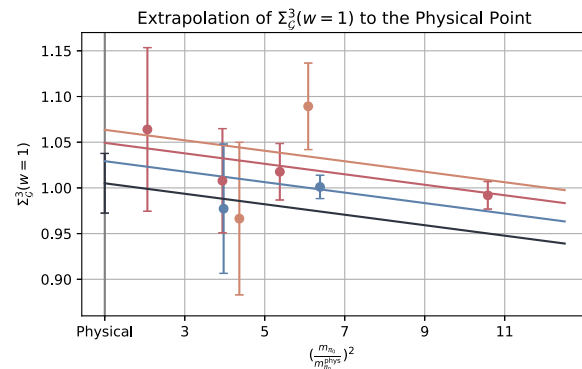
FIG. 8. Visualization of the extrapolation to the physical point of the ratio $\Sigma_{\mathcal{G}}^i(w=1)$ using Eq. (4.1) for two different mass step-scaling steps.
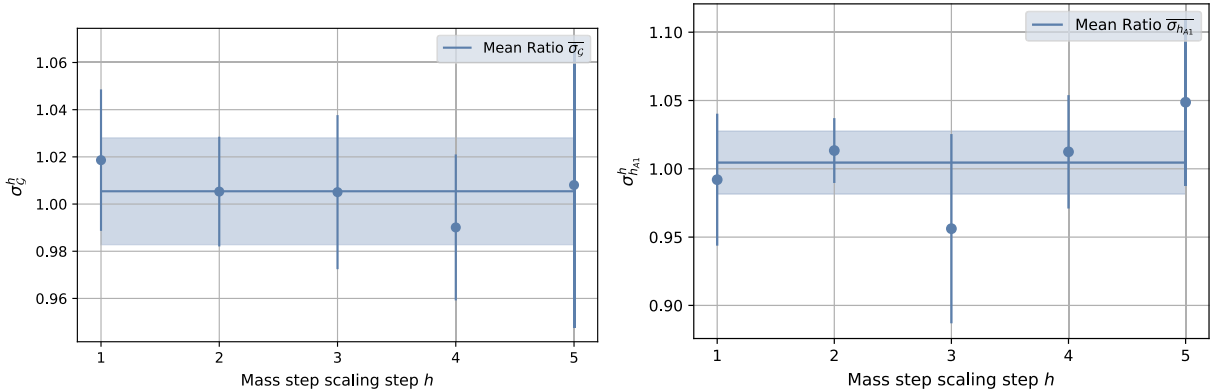
FIG. 9. Average ratio of successive $\mathcal{G}$ (left) and h_{A_1} (right) at the physical point.
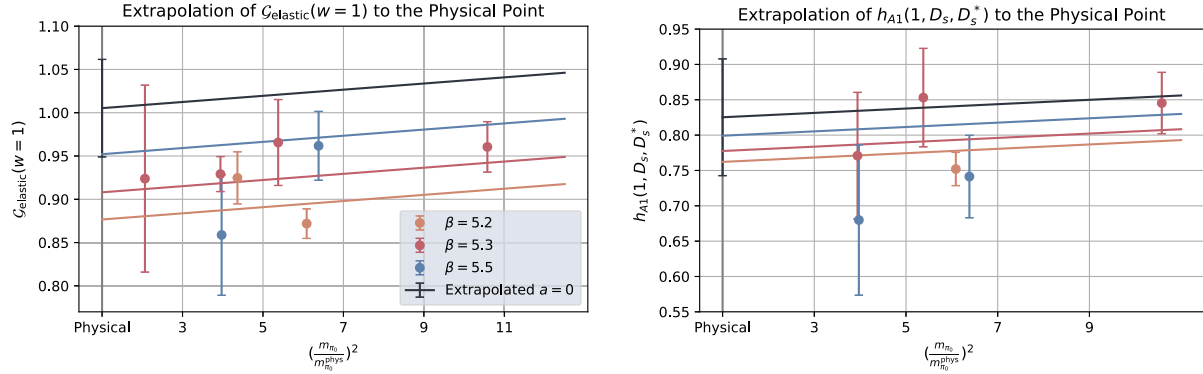
FIG. 10. Visualization of the combined fit Eq. (4.3) and extrapolation to the physical point for $\mathcal{G}_{\text{elastic}}$ (left) and $h_{A_1}(D_s, D_s^*)$ (right).

$$\Sigma_{\mathcal{G}}(w = 1, a, m_\pi, m_{H_s}) = \Sigma_{\mathcal{G}_0} + \Sigma_{\mathcal{G}_1} \times (a/a_{\beta=5.3})^2$$
$$+ \Sigma_{\mathcal{G}_2} \times \left(\frac{m_\pi}{m_\pi^{\text{physical}}}\right)^2 + \Sigma_{\mathcal{G}_3} \times (r_{\text{mis}} - 1)$$
$$+ \Sigma_{\mathcal{G}_4} \times \frac{m_{B_s}}{m_{H_s}}, \tag{4.5}$$

where r_{mis} is defined as $\frac{a m_{H_s}}{\lambda^i a m_{D_s}}$, and m_{H_s} denotes the physical meson mass. While the mistuning is not significant, $\Sigma_{\mathcal{G}_3} = 0.69(71)$, an inclusion of this term makes the fit less stable. The last term does contribute $\Sigma_{\mathcal{G}_4} = -0.0248(91)$, but the ratios (analogous to Fig. 9) are still compatible with a constant. We obtain a final result for this method by computing

$$\prod_{h=1}^{6} \Sigma_{\mathcal{G}}(w = 1, a = 0, m_\pi = m_\pi^{\text{phys}}, m_{D_s}\lambda^i) = 1.03(14). \tag{4.6}$$

Coincidently, we get the same result as we get with the individual fits.

The extrapolation of h_{A_1} to the physical point is completely analogous to that of $\mathcal{G}$. We have decided to use individual fits as we did for the extrapolation of $\mathcal{G}$. First, we use the ansatz

$$h_{A_1}{}^{\text{lat}}(w = 1, a, m_\pi^2, m_{D_s}) = h_{A_1}^0 + h_{A_1}^1 (m_\pi/m_\pi^{\text{physical}})^2$$
$$+ h_{A_1}^2 (a/a_{\beta=5.3})^2 \tag{4.7}$$

to get $h_{A_1}^{D_s \to D_s^*}(1)$ as shown in the right panel of Fig. 10. Then, the ratios of successive mass step-scaling steps are fitted with

$$\Sigma_{h_{A_1}}^i (1, a, m_\pi^2) = \Sigma_{h_{A_1}}^{i,0} + \Sigma_{h_{A_1}}^{i,1} \times (a/a_{\beta=5.3})^2$$
$$+ \Sigma_{h_{A_1}}^{i,2} \times \left(\frac{m_\pi}{m_\pi^{\text{physical}}}\right)^2. \tag{4.8}$$

The fit results are listed in Table IV.

Again, the pion mass dependence is very weak, below 1%. It is less straightforward to conclude about cutoff effects. They seem to be more significant than for $\Sigma_{\mathcal{G}}^i$, as large as 12%. As for $\Sigma_{\mathcal{G}}^i$, adding a mistuning term $(1 - \frac{m_{H_s}}{\lambda^i m_{D_s}})$ has made the fits unstable. In the same way as before, from the ratios at the physical point and in the continuum limit, a fit to a constant $\bar{\sigma}_{h_{A_1}}$ of the ratios $\sigma_{h_{A_1}}^i$ is performed, because again no clear trend in m_{H_s} is observed as shown in the right panel of Fig. 9. The result for h_{A_1} can now be calculated according to Eq. (2.24),

$$h_{A_1}^{B_s \to D_s^*}(1) = h_{A_1}^{D_s \to D_s^*}(1) \times (\bar{\sigma}_{h_{A_1}})^K$$
$$= 0.825(83) \times (1.005(23))^6 = 0.85(16). \tag{4.9}$$

C. Discussion

To our knowledge, only three lattice results for $\mathcal{G}^{B_s \to D_s}(1)$ are quoted in the literature. The ETM Collaboration, in their analysis of ensembles with $N_f = 2$

TABLE IV. Fit parameters for the extrapolation of $\Sigma_{h_{A_1}}^i$.

I	$\Sigma_{h_{A_1}}^{i,0}$	$\Sigma_{h_{A_1}}^{i,1}$	$\Sigma_{h_{A_1}}^{i,2}$	$\chi^2/\text{d.o.f.}$
1	0.993(50)	−0.002(38)	−0.0011(24)	0.56485
2	1.015(26)	−0.007(19)	−0.0018(26)	0.47967
3	0.958(72)	0.081(74)	−0.0022(63)	1.08455
4	1.013(44)	0.008(31)	−0.0005(39)	0.11045
5	1.038(66)	−0.125(90)	0.010(10)	0.26381
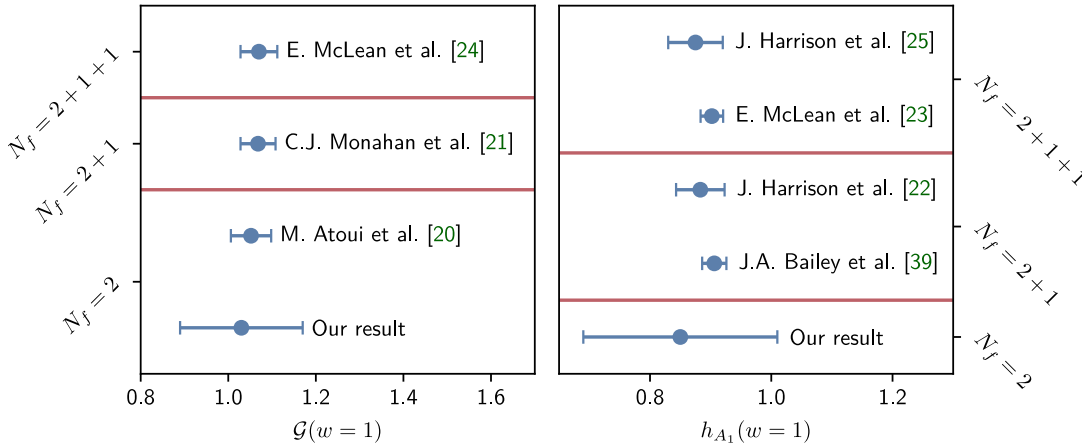
FIG. 11. Comparison to previous results for $\mathcal{G}(w = 1)$ (left) and h_{A_1} (right).

twisted-mass fermions, gets $\mathcal{G}^{B_s \to D_s}(1) = 1.052(46)$, using the step scaling in mass method defined through RGI quark masses [20]. The HPQCD Collaboration has analyzed ensembles with $N_f = 2 + 1$ staggered fermions, using the nonrelativistic framework to regularize the b quark. The result reads $\mathcal{G}^{B_s \to D_s}(1) = 1.068(40)$ [21]. They have also analyzed ensembles with $N_f = 2 + 1 + 1$ staggered fermions, regularizing the b quark with the heavy HISQ action [24]: they get $\mathcal{G}^{B_s \to D_s}(1) = 1.070(42)$.[3] Our result is in the same ballpark as the three previous lattice computations, with a significantly larger error.[4] A possible explanation is that we have set a large source-sink time separation $\gtrsim 2$ fm. This conservative choice helps to reduce the contamination from excited states with the caveat that the signal deteriorates faster for correlators build from heavy quarks.

Let us emphasize that a gain in statistics at each individual point of the step scaling in mass strategy would have a significant impact to reduce the error on the final result, because the individual errors multiply with each other along the steps.

Three lattice results have been quoted in the literature for $h_{A_1}^{B_s \to D_s^*}(1)$ by the HPQCD Collaboration at $N_f = 2 + 1$ and $N_f = 2 + 1 + 1$. Using a nonrelativistic b quark, again, they get $h_{A_1}^{B_s \to D_s^*}(1) = 0.883(40)$ [22], while in the heavy HISQ framework, they get $h_{A_1}^{B_s \to D_s^*}(1) = 0.9020(96)(90)$ [23] by a measurement directly at zero recoil and $h_{A_1}^{B_s \to D_s^*} = 0.875(45)$ [25] by extrapolation to zero recoil. The authors of [22] find a tiny dependence on the spectator quark mass $(h_{A_1}^{B \to D^*}/h_{A_1}^{B_s \to D_s^*} = 1.013(31))$. The FNAL/MILC

Collaboration finds from another set of ensembles with $N_f = 2 + 1$ staggered fermions, $h_{A_1}^{B \to D^*}(1) = 0.906(20)$, using the Fermilab action to regularize the b quark [39]. Two more recent preliminaries studies by this collaboration state $h_{A_1}^{B \to D^*}(1) \in [0.90, 0.95]$ [40,41]. Thus, there is convincing evidence that $h_{A_1}^{B_s \to D_s^*}(1) \sim 0.9$. The same remark concerning our statistical error can be made for $h_{A_1}^{B_s \to D_s^*}$ as we did for $\mathcal{G}^{B_s \to D_s}(1)$. The value of the "elastic" point $h_{A_1}^{D_s \to D_s^*}(1)$ leads to the conclusion that heavy quark mass dependence on this form factor is smaller than 10%, as it is for $\mathcal{G}^{H_s \to D_s}(1)$.

V. CONCLUSION

A comparison to previous results is shown in Fig. 11. In the present paper, we have reported an $N_f = 2$ lattice QCD computation of the form factors $\mathcal{G}(1)$ and $h_{A_1}(1)$ associated to the $B_s \to D_s^{(*)} l\nu$ semileptonic decays. For the purpose of extracting the underlying heavy-heavy hadronic matrix elements from suitable correlators, we have clearly demonstrated that solving the GEVP is beneficial to reduce their contamination by excited states. Yet, only smearing $D_s^{(*)}$ and B_s interpolating fields is already a good starting point. Step scaling in masses helps to control cutoff effects originating from the heavy quark regularized on the lattice with the Wilson-Clover action. The twisted-boundary condition technique proves to be very helpful to extrapolate $\mathcal{G}(w)$ at zero recoil. It allows us to consider kinematics near-zero recoil so that a linear extrapolation in $(w - 1)$ is fully satisfactory. As we were conservative in setting the source-sink time separation larger than 2 fm in three-point correlation functions, we end up with statistical errors $\sim 2.5\%$ in the heavy-strange meson masses sequence of form factor ratios. This precision is not yet sufficient to be sensitive to the heavy quark mass dependence and thus also

---

[3]We thank Jonna Koponen for having provided us with the value that is not explicitly quoted in [24].

[4]The authors of [20] quote the same order of statistics for their matrix elements but a much smaller error in their extrapolation.

entails the still considerably large overall errors of the form factors from the present pilot study.

From the findings of our study, it can be deduced that a significant improvement in precision can be expected from a reduced, less conservative choice for the source-sink time separation and focusing on the most smeared sources, on top of generally higher statistics of the individual ensembles of gauge field configurations that enter the analysis. However, rather than pursuing this for the two-flavor theory which is known to have only limited impact on precision phenomenology, we intend to take these aspects into account in a future calculation of $B_s \to D_s^{(*)}$ form factors using lattice QCD ensembles with $N_f = 2 + 1$ dynamical quarks in the medium term. In fact, thanks again to large-scale simulations carried out by the CLS cooperation of researchers,[5] a rich landscape of such $(2 + 1)$-flavor gauge field configuration ensembles is already available [42–44], which are to be regarded as natural successors to the ones investigated in the present work. These ensembles employ nonperturbatively $O(a)$ improved Wilson-Clover fermions, together with the tree-level Symanzik-improved gauge action, and cover lattice spacings close to the continuum limit as well as the physical pion mass point. Since they also offer statistics substantially higher than underlying our $N_f = 2$ analysis, a computationally feasible application of the methods studied (and its extensions suggested) here to the $N_f = 2 + 1$ case, including additional form factors of the B_s system, now appears realistic. Therefore, even though the cost of large-volume calculations via the step scaling in mass strategy remains challenging, an outcome of phenomenologically interesting target precision of a few percent may be accomplished from this approach on a reasonable time scale.

Finally, let us also mention the recently proposed, so-called stabilized Wilson fermions as a new avenue for QCD calculations with (improved) Wilson-type fermions [45]. First, simulations of lattice QCD with $2 + 1$ dynamical quark flavors within this formulation [46], which amounts to replacing the original clover term with an exponentiated version of it, already hint at improved properties such as,

apart from stabilizing simulations in large volumes towards small pion masses, an overall good continuum scaling and milder relative quark mass dependent cutoff effects. Hence, this framework brings into sight another promising direction for estimating strong interaction effects in precision weak interaction phenomenology through lattice QCD that we are also envisaging for future applications of the techniques explored in the present study.

APPENDIX: INTERMEDIATE RESULTS

In Tables V–XXXIV, we collect intermediate results of our analysis.

TABLE V. Pseudoscalar masses on A5.

κ_h	Range	am_p
0.12531	[8, 24]	0.74953(64)
0.121364	[8, 22]	0.88547(91)
0.11604	[6, 20]	1.04906(68)
0.109307	[7, 25]	1.23385(71)
0.100407	[8, 20]	1.45746(88)
0.089288	[6, 17]	1.71981(79)

---

[5]https://www.zeuthen.desy.de/alpha/public-cls-nf21/.

TABLE VI. Improved and renormalized hadronic matrix elements $\langle D_s | V_\mu | H_s \rangle$ on A5.

κ_h	θ	Range	V_0^I	V_0^{IR}	Range	V_n^I	V_n^{IR}
0.12531	0	[8, 29]	1.353(27)	1.315(26)	[17, 29]	0.0032(15)	0.0031(15)
0.12531	0.15	[5, 28]	1.392(48)	1.352(47)	[15, 29]	0.0185(55)	0.0180(53)
0.12531	0.3	[6, 28]	1.385(47)	1.345(46)	[10, 32]	0.0263(45)	0.0255(44)
0.12531	0.525	[6, 27]	1.336(46)	1.298(44)	[10, 31]	0.0443(47)	0.0430(46)
0.12531	0.75	[7, 27]	1.327(49)	1.290(47)	[10, 30]	0.0631(53)	0.0613(52)
0.12531	1.05	[5, 26]	1.295(53)	1.258(52)	[18, 31]	0.0859(73)	0.0834(71)
0.12531	1.275	[6, 28]	1.281(57)	1.245(56)	[12, 30]	0.1043(78)	0.1014(76)
0.121364	0	[5, 26]	1.385(29)	1.407(29)	[17, 30]	0.0029(14)	0.0030(14)
0.121364	0.15	[6, 29]	1.424(53)	1.446(54)	[11, 29]	0.0172(50)	0.0175(51)
0.121364	0.3	[9, 30]	1.413(50)	1.436(50)	[8, 28]	0.0306(52)	0.0311(53)
0.121364	0.525	[8, 28]	1.373(50)	1.395(51)	[11, 31]	0.0441(50)	0.0448(50)
0.121364	0.75	[7, 28]	1.364(53)	1.386(54)	[10, 30]	0.0640(57)	0.0650(58)
0.121364	1.05	[5, 27]	1.315(60)	1.336(61)	[9, 29]	0.0904(69)	0.0919(70)
0.121364	1.275	[3, 27]	1.301(63)	1.322(64)	[11, 30]	0.1089(81)	0.1107(82)
0.11604	0	[7, 29]	1.400(30)	1.513(33)	[16, 31]	0.0031(14)	0.0033(15)
0.11604	0.15	[4, 29]	1.440(58)	1.555(63)	[9, 28]	0.0178(53)	0.0192(58)
0.11604	0.3	[17, 31]	1.419(49)	1.533(53)	[10, 27]	0.0319(60)	0.0344(64)
0.11604	0.525	[6, 29]	1.397(53)	1.508(57)	[13, 30]	0.0433(54)	0.0468(59)
0.11604	0.75	[6, 29]	1.386(56)	1.497(60)	[11, 30]	0.0640(60)	0.0692(65)
0.11604	1.05	[6, 27]	1.320(67)	1.425(73)	[10, 29]	0.0935(75)	0.1009(81)
0.11604	1.275	[6, 29]	1.301(72)	1.405(78)	[12, 28]	0.1113(92)	0.1202(99)
0.109307	0	[7, 28]	1.443(38)	1.687(44)	[11, 28]	0.0050(22)	0.0059(25)
0.109307	0.15	[3, 30]	1.457(65)	1.704(76)	[16, 28]	0.0283(62)	0.0331(73)
0.109307	0.3	[4, 29]	1.449(66)	1.694(77)	[14, 28]	0.0421(64)	0.0492(75)
0.109307	0.525	[6, 29]	1.440(59)	1.684(69)	[11, 31]	0.0470(57)	0.0550(66)
0.109307	0.75	[4, 30]	1.437(61)	1.681(71)	[10, 31]	0.0659(63)	0.0770(74)
0.109307	1.05	[4, 30]	1.428(77)	1.671(91)	[10, 28]	0.0807(82)	0.0944(96)
0.109307	1.275	[6, 30]	1.419(83)	1.659(98)	[10, 28]	0.0962(96)	0.113(11)
0.100407	0	[10, 29]	1.403(35)	1.833(46)	[12, 28]	0.0055(21)	0.0072(27)
0.100407	0.15	[9, 30]	1.415(62)	1.848(80)	[14, 29]	0.0268(59)	0.0351(77)
0.100407	0.3	[10, 30]	1.404(61)	1.833(80)	[14, 29]	0.0396(62)	0.0518(81)
0.100407	0.525	[11, 30]	1.399(55)	1.828(72)	[10, 30]	0.0466(61)	0.0609(80)
0.100407	0.75	[10, 30]	1.398(58)	1.826(76)	[9, 31]	0.0661(63)	0.0863(82)
0.100407	1.05	[10, 29]	1.406(78)	1.84(10)	[10, 27]	0.0771(90)	0.101(12)
0.100407	1.275	[10, 31]	1.400(84)	1.83(11)	[11, 28]	0.094(10)	0.123(14)
0.089288	0	[13, 29]	1.309(30)	1.988(46)	[15, 32]	0.0030(14)	0.0046(21)
0.089288	0.15	[16, 30]	1.332(48)	2.023(72)	[13, 27]	0.0103(74)	0.016(11)
0.089288	0.3	[14, 28]	1.332(53)	2.023(81)	[13, 29]	0.0190(60)	0.0288(91)
0.089288	0.525	[16, 30]	1.350(53)	2.051(81)	[18, 29]	0.0395(62)	0.0600(95)
0.089288	0.75	[17, 32]	1.347(54)	2.046(82)	[12, 29]	0.0628(70)	0.095(11)
0.089288	1.05	[17, 31]	1.228(57)	1.866(87)	[13, 30]	0.0872(74)	0.132(11)
0.089288	1.275	[18, 30]	1.214(65)	1.843(98)	[11, 29]	0.1009(93)	0.153(14)

TABLE VII. h_{A_1} extracted on ensemble A5.

κ_h	Range	$\langle D_s^* | \vec{A}^I | H_s \rangle_{\parallel}^R$	h_{A_1}	$\Sigma_{h_{A_1}}$
0.12531	[6, 24]	1.204(38)	0.752(24)	$\cdots$
0.121364	[7, 25]	1.229(44)	0.739(26)	0.983(12)
0.11604	[7, 23]	1.247(51)	0.732(30)	0.991(11)
0.109307	[8, 27]	1.400(64)	0.820(37)	1.121(65)
0.100407	[11, 27]	1.391(74)	0.838(45)	1.022(14)
0.089288	[19, 31]	1.206(81)	0.777(52)	0.928(75)

TABLE VIII. $\mathcal{G}$ at zero recoil and $\Sigma_i = \frac{\mathcal{G}_i}{\mathcal{G}_{i-1}}$ on A5.

Scaling step	$\mathcal{G}(w=1)$	$\Sigma_{\mathcal{G}}$
D_s	0.872(17)	. . .
1	0.862(23)	0.9890(10)
2	0.848(26)	0.98289(81)
3	0.923(39)	1.0893(29)
4	0.932(48)	1.00921(92)
5	0.850(51)	0.9124(46)

TABLE IX. Pseudoscalar masses on B6.

κ_h	Range	am_p
0.12529	[11, 37]	0.74884(34)
0.121313	[11, 37]	0.88526(48)
0.116844	[12, 34]	1.02281(57)
0.109127	[8, 27]	1.23825(51)
0.100172	[7, 23]	1.46300(53)
0.088934	[8, 20]	1.72617(57)

TABLE X. Improved and renormalized hadronic matrix elements $\langle D_s|V_\mu|H_s\rangle$ on B6.

κ_h	θ	Range	V_0^I	V_0^{IR}	Range	V_n^I	V_n^{IR}
0.12529	0	[9, 40]	1.406(48)	1.367(47)	[14, 45]	0.0045(19)	0.0044(19)
0.12529	0.163	[7, 44]	1.424(46)	1.384(45)	[12, 46]	0.0091(37)	0.0089(36)
0.12529	0.326	[9, 44]	1.425(41)	1.386(40)	[9, 46]	0.0169(61)	0.0164(60)
0.12529	0.5705	[6, 42]	1.403(52)	1.364(51)	[14, 48]	0.0270(70)	0.0262(68)
0.12529	0.815	[7, 40]	1.398(53)	1.359(52)	[12, 47]	0.0377(68)	0.0367(66)
0.12529	1.14095	[15, 45]	1.369(53)	1.331(51)	[9, 43]	0.0713(73)	0.0693(71)
0.12529	1.38545	[13, 45]	1.361(53)	1.323(51)	[15, 42]	0.0844(83)	0.0821(81)
0.121313	0	[8, 41]	1.433(54)	1.458(55)	[14, 45]	0.0059(28)	0.0060(28)
0.121313	0.163	[10, 44]	1.454(50)	1.478(51)	[15, 46]	0.0113(54)	0.0115(55)
0.121313	0.326	[7, 44]	1.455(47)	1.480(48)	[14, 46]	0.0186(72)	0.0189(74)
0.121313	0.5705	[9, 42]	1.434(55)	1.458(56)	[15, 46]	0.0272(75)	0.0277(77)
0.121313	0.815	[7, 43]	1.430(59)	1.454(60)	[9, 45]	0.0376(75)	0.0383(77)
0.121313	1.14095	[15, 45]	1.393(61)	1.417(62)	[10, 44]	0.0757(88)	0.0769(89)
0.121313	1.38545	[21, 46]	1.373(71)	1.396(73)	[9, 43]	0.0895(98)	0.0910(100)
0.116844	0	[16, 44]	1.440(57)	1.556(62)	[20, 45]	0.0073(34)	0.0079(37)
0.116844	0.163	[16, 44]	1.465(54)	1.583(58)	[22, 43]	0.0134(89)	0.0145(96)
0.116844	0.326	[16, 45]	1.467(50)	1.585(54)	[20, 45]	0.022(10)	0.024(11)
0.116844	0.5705	[14, 45]	1.444(59)	1.560(64)	[19, 46]	0.0284(77)	0.0307(83)
0.116844	0.815	[15, 44]	1.440(65)	1.555(71)	[17, 45]	0.0391(92)	0.0423(99)
0.116844	1.14095	[18, 46]	1.399(72)	1.511(77)	[17, 44]	0.078(10)	0.084(11)
0.116844	1.38545	[21, 45]	1.384(82)	1.495(89)	[15, 42]	0.091(12)	0.098(13)
0.109127	0	[21, 45]	1.393(48)	1.633(56)	[24, 46]	0.0033(24)	0.0039(28)
0.109127	0.163	[29, 46]	1.402(49)	1.644(57)	[29, 47]	0.0047(49)	0.0055(58)
0.109127	0.326	[25, 45]	1.392(52)	1.632(61)	[26, 45]	0.0123(85)	0.0144(99)
0.109127	0.5705	[21, 46]	1.402(54)	1.644(64)	[24, 48]	0.0395(77)	0.0464(90)
0.109127	0.815	[22, 45]	1.402(61)	1.644(71)	[28, 47]	0.0529(89)	0.062(10)
0.109127	1.14095	[26, 45]	1.382(67)	1.621(79)	[15, 39]	0.056(15)	0.065(18)
0.109127	1.38545	[31, 45]	1.378(74)	1.616(87)	[20, 43]	0.070(13)	0.082(16)
0.100172	0	[25, 47]	1.356(44)	1.781(58)	[29, 48]	0.0037(25)	0.0049(32)
0.100172	0.163	[31, 46]	1.370(47)	1.799(62)	[32, 47]	0.0069(56)	0.0091(73)
0.100172	0.326	[27, 46]	1.359(51)	1.785(66)	[24, 41]	0.017(13)	0.022(17)
0.100172	0.5705	[25, 46]	1.371(53)	1.800(70)	[28, 48]	0.0418(81)	0.055(11)
0.100172	0.815	[25, 46]	1.369(60)	1.798(79)	[29, 47]	0.0536(91)	0.070(12)
0.100172	1.14095	[26, 45]	1.355(69)	1.780(90)	[24, 43]	0.052(13)	0.069(17)
0.100172	1.38545	[33, 46]	1.346(73)	1.768(96)	[25, 45]	0.073(12)	0.096(16)
0.088934	0	[29, 46]	1.291(40)	1.982(61)	[30, 48]	0.0022(23)	0.0034(35)
0.088934	0.163	[31, 45]	1.324(44)	2.032(67)	[28, 45]	0.0156(97)	0.024(15)
0.088934	0.326	[32, 46]	1.328(44)	2.038(67)	[26, 40]	0.025(13)	0.039(19)
0.088934	0.5705	[32, 45]	1.311(54)	2.013(83)	[34, 49]	0.0245(73)	0.038(11)
0.088934	0.815	[33, 46]	1.308(57)	2.009(87)	[36, 47]	0.0398(83)	0.061(13)
0.088934	1.14095	[37, 47]	1.183(59)	1.816(90)	[21, 40]	0.072(22)	0.110(33)
0.088934	1.38545	[37, 47]	1.149(72)	1.76(11)	[29, 46]	0.076(13)	0.117(20)

TABLE XI. $\mathcal{G}$ at zero recoil and $\Sigma_i = \frac{\mathcal{G}_i}{\mathcal{G}_{i-1}}$ on B6.

Scaling step	$\mathcal{G}(w = 1)$	$\Sigma_{\mathcal{G}}$
D_s	0.925(30)	...
1	0.895(41)	0.96727(89)
2	0.878(53)	0.98133(78)
3	0.848(60)	0.9664(31)
4	0.895(76)	1.0551(10)
5	0.847(89)	0.9459(45)

TABLE XII. Pseudoscalar masses on E5.

κ_h	Range	am_p
0.12724	[9, 25]	0.65743(80)
0.123874	[8, 27]	0.7765(10)
0.119457	[9, 27]	0.9166(11)
0.113638	[7, 27]	1.0835(12)
0.106031	[7, 22]	1.2813(13)
0.0965545	[8, 17]	1.5084(16)

TABLE XIII. Improved and renormalized hadronic matrix elements $\langle D_s | V_\mu | H_s \rangle$ on E5.

κ_h	θ	Range	V_0^I	V_0^{IR}	Range	V_n^I	V_n^{IR}
0.12724	0	[5, 29]	1.325(43)	1.261(41)	[7, 32]	0.0037(20)	0.0035(19)
0.12724	0.125	[7, 27]	1.331(41)	1.266(40)	[5, 29]	0.0115(39)	0.0110(37)
0.12724	0.25	[5, 27]	1.340(42)	1.275(40)	[8, 29]	0.0232(41)	0.0221(39)
0.12724	0.4375	[6, 28]	1.365(43)	1.299(41)	[5, 30]	0.0427(44)	0.0407(42)
0.12724	0.625	[4, 29]	1.403(45)	1.335(43)	[9, 27]	0.0609(52)	0.0580(49)
0.12724	0.875	[4, 30]	1.465(51)	1.394(48)	[11, 30]	0.0863(65)	0.0821(62)
0.12724	1.0625	[5, 28]	1.528(56)	1.454(53)	[12, 29]	0.1078(75)	0.1026(71)
0.123874	0	[5, 28]	1.368(46)	1.354(46)	[4, 30]	0.0040(21)	0.0039(21)
0.123874	0.125	[5, 26]	1.374(45)	1.360(45)	[10, 32]	0.0108(42)	0.0107(41)
0.123874	0.25	[6, 28]	1.384(45)	1.369(44)	[5, 28]	0.0253(48)	0.0250(47)
0.123874	0.4375	[4, 28]	1.409(46)	1.394(46)	[7, 28]	0.0446(52)	0.0441(52)
0.123874	0.625	[4, 29]	1.449(48)	1.433(48)	[9, 28]	0.0642(59)	0.0635(58)
0.123874	0.875	[4, 28]	1.513(55)	1.497(54)	[10, 29]	0.0912(70)	0.0902(69)
0.123874	1.0625	[5, 27]	1.578(60)	1.561(59)	[12, 30]	0.1128(78)	0.1116(77)
0.119457	0	[5, 29]	1.397(52)	1.454(54)	[10, 31]	0.0033(26)	0.0035(28)
0.119457	0.125	[5, 28]	1.404(50)	1.461(52)	[12, 29]	0.0109(47)	0.0113(49)
0.119457	0.25	[5, 27]	1.414(51)	1.472(53)	[12, 30]	0.0242(47)	0.0252(49)
0.119457	0.4375	[5, 30]	1.439(51)	1.497(53)	[7, 29]	0.0461(56)	0.0480(58)
0.119457	0.625	[5, 30]	1.480(54)	1.540(56)	[12, 29]	0.0663(62)	0.0690(65)
0.119457	0.875	[4, 29]	1.545(62)	1.608(64)	[10, 29]	0.0953(75)	0.0992(78)
0.119457	1.0625	[5, 28]	1.613(68)	1.678(71)	[14, 30]	0.1192(88)	0.1241(92)
0.113638	0	[8, 29]	1.412(52)	1.572(58)	[10, 31]	0.0034(34)	0.0037(38)
0.113638	0.125	[6, 27]	1.422(54)	1.583(60)	[11, 30]	0.0108(46)	0.0120(51)
0.113638	0.25	[7, 27]	1.431(53)	1.594(60)	[10, 30]	0.0247(49)	0.0275(55)
0.113638	0.4375	[4, 30]	1.454(53)	1.619(60)	[10, 30]	0.0460(56)	0.0512(63)
0.113638	0.625	[4, 28]	1.497(58)	1.667(65)	[12, 29]	0.0685(67)	0.0762(74)
0.113638	0.875	[6, 28]	1.563(65)	1.740(72)	[9, 30]	0.0981(72)	0.1093(80)
0.113638	1.0625	[5, 29]	1.631(72)	1.817(81)	[12, 30]	0.1221(91)	0.136(10)
0.106031	0	[10, 30]	1.396(54)	1.703(65)	[10, 29]	0.0039(44)	0.0047(54)
0.106031	0.125	[11, 29]	1.405(53)	1.713(65)	[12, 30]	0.0108(46)	0.0131(56)
0.106031	0.25	[10, 29]	1.414(54)	1.725(66)	[11, 30]	0.0248(49)	0.0302(60)
0.106031	0.4375	[12, 29]	1.439(54)	1.756(66)	[11, 29]	0.0463(60)	0.0565(73)
0.106031	0.625	[13, 30]	1.480(56)	1.806(69)	[11, 30]	0.0684(66)	0.0835(80)
0.106031	0.875	[11, 30]	1.545(66)	1.884(81)	[11, 30]	0.0986(77)	0.1203(94)
0.106031	1.0625	[12, 29]	1.615(76)	1.970(93)	[11, 30]	0.1232(96)	0.150(12)
0.0965545	0	[14, 29]	1.351(54)	1.858(74)	[13, 30]	0.0037(37)	0.0051(51)
0.0965545	0.125	[14, 30]	1.356(51)	1.866(71)	[10, 29]	0.0102(48)	0.0140(66)
0.0965545	0.25	[14, 31]	1.366(50)	1.879(69)	[8, 26]	0.0226(71)	0.0311(97)
0.0965545	0.4375	[14, 30]	1.391(53)	1.913(73)	[14, 30]	0.0457(55)	0.0629(76)
0.0965545	0.625	[14, 30]	1.432(57)	1.970(78)	[13, 29]	0.0680(70)	0.0936(97)
0.0965545	0.875	[14, 30]	1.492(66)	2.053(90)	[7, 29]	0.0964(85)	0.133(12)
0.0965545	1.0625	[14, 30]	1.560(76)	2.15(10)	[6, 30]	0.1182(99)	0.163(14)

TABLE XIV. h_{A_1} extracted on Ensemble E5.

κ_h	Range	$\langle D_s^* | \vec{A}^I | H_s \rangle_\parallel^R$	h_{A_1}	$\Sigma_{h_{A1}}$
0.12724	[10, 23]	1.212(63)	0.845(43)	$\cdots$
0.123874	[8, 20]	1.240(68)	0.828(44)	0.9791(91)
0.119457	[8, 18]	1.271(78)	0.821(50)	0.992(12)
0.113638	[9, 20]	1.310(91)	0.833(57)	1.015(19)
0.106031	[10, 23]	1.32(11)	0.847(67)	1.016(18)
0.0965545	[14, 29]	1.30(11)	0.866(72)	1.023(22)

TABLE XV. $\mathcal{G}$ at zero recoil and $\Sigma_i = \frac{\mathcal{G}_i}{\mathcal{G}_{i-1}}$ on E5.

Scaling step	$\mathcal{G}(w = 1)$	$\Sigma_{\mathcal{G}}$
D_s	0.961(29)	$\cdots$
1	0.945(32)	0.9842(11)
2	0.930(39)	0.98338(98)
3	0.922(57)	0.9919(10)
4	0.919(67)	0.9971(11)
5	0.929(81)	1.0100(13)

TABLE XVI. Pseudoscalar masses on F6.

κ_h	Range	am_p
0.12713	[12, 39]	0.65756(70)
0.1237	[10, 35]	0.77899(69)
0.119241	[10, 34]	0.91989(79)
0.113382	[7, 27]	1.08818(74)
0.10593	[8, 22]	1.28429(94)
0.096211	[5, 18]	1.51684(82)

TABLE XVII. Improved and renormalized hadronic matrix elements $\langle D_s | V_\mu | H_s \rangle$ on F6.

κ_h	θ	Range	V_0^I	V_0^{IR}	Range	V_n^I	V_n^{IR}
0.12713	0	[5, 43]	1.335(68)	1.270(65)	[13, 45]	0.0057(33)	0.0054(31)
0.12713	0.1875	[6, 43]	1.344(68)	1.279(65)	[13, 45]	0.0106(58)	0.0100(55)
0.12713	0.375	[9, 44]	1.332(71)	1.268(68)	[16, 44]	0.0230(59)	0.0219(57)
0.12713	0.65625	[12, 44]	1.337(72)	1.272(69)	[15, 44]	0.0424(64)	0.0403(61)
0.12713	0.9375	[15, 44]	1.343(76)	1.278(73)	[17, 41]	0.0635(81)	0.0604(77)
0.12713	1.3125	[17, 46]	1.358(88)	1.293(84)	[15, 44]	0.0881(91)	0.0838(87)
0.12713	1.59375	[23, 46]	1.37(11)	1.31(10)	[14, 45]	0.107(11)	0.102(10)
0.1237	0	[14, 45]	1.383(76)	1.369(75)	[14, 46]	0.0050(25)	0.0050(25)
0.1237	0.1875	[8, 45]	1.398(79)	1.384(78)	[16, 43]	0.0133(65)	0.0132(65)
0.1237	0.375	[13, 44]	1.378(79)	1.364(79)	[15, 42]	0.0271(69)	0.0268(68)
0.1237	0.65625	[14, 45]	1.379(81)	1.365(80)	[16, 41]	0.0482(78)	0.0477(78)
0.1237	0.9375	[24, 46]	1.375(85)	1.361(84)	[14, 43]	0.0671(82)	0.0664(81)
0.1237	1.3125	[23, 44]	1.39(10)	1.371(99)	[16, 45]	0.094(10)	0.0932(100)
0.1237	1.59375	[26, 46]	1.40(12)	1.39(12)	[13, 43]	0.114(12)	0.113(12)
0.119241	0	[20, 44]	1.403(81)	1.462(84)	[20, 48]	0.0056(31)	0.0059(33)
0.119241	0.1875	[16, 44]	1.418(85)	1.478(88)	[20, 42]	0.0176(75)	0.0183(78)
0.119241	0.375	[21, 46]	1.392(83)	1.451(86)	[20, 42]	0.0312(78)	0.0325(81)
0.119241	0.65625	[20, 45]	1.392(87)	1.451(90)	[20, 41]	0.0529(91)	0.0551(95)
0.119241	0.9375	[21, 45]	1.393(93)	1.451(97)	[20, 41]	0.074(10)	0.077(11)
0.119241	1.3125	[23, 46]	1.40(11)	1.46(11)	[19, 43]	0.101(12)	0.105(13)
0.119241	1.59375	[23, 45]	1.41(13)	1.47(13)	[18, 44]	0.120(15)	0.125(16)
0.113382	0	[23, 45]	1.414(81)	1.576(90)	[28, 48]	0.0062(41)	0.0069(46)
0.113382	0.1875	[25, 46]	1.427(81)	1.590(90)	[26, 44]	0.0181(70)	0.0202(78)
0.113382	0.375	[25, 47]	1.399(81)	1.559(90)	[28, 42]	0.0337(85)	0.0376(95)
0.113382	0.65625	[27, 47]	1.398(83)	1.558(93)	[27, 42]	0.0556(97)	0.062(11)
0.113382	0.9375	[26, 45]	1.399(93)	1.56(10)	[28, 44]	0.0747(99)	0.083(11)
0.113382	1.3125	[27, 46]	1.40(11)	1.56(12)	[21, 44]	0.105(14)	0.117(15)
0.113382	1.59375	[27, 45]	1.42(14)	1.58(15)	[36, 47]	0.116(18)	0.130(20)

(Table continued)

TABLE XVII. *(Continued)*

κ_h	θ	Range	V_0^I	V_0^{IR}	Range	V_n^I	V_n^{IR}
0.10593	0	[31, 46]	1.337(67)	1.640(82)	[26, 46]	0.0051(22)	0.0063(27)
0.10593	0.1875	[31, 47]	1.361(68)	1.669(83)	[23, 45]	0.0132(57)	0.0162(70)
0.10593	0.375	[29, 46]	1.346(77)	1.651(94)	[35, 45]	0.0282(69)	0.0346(85)
0.10593	0.65625	[33, 45]	1.354(79)	1.661(97)	[34, 48]	0.0462(70)	0.0567(86)
0.10593	0.9375	[34, 47]	1.367(90)	1.68(11)	[24, 46]	0.0634(89)	0.078(11)
0.10593	1.3125	[34, 47]	1.41(11)	1.73(13)	[32, 45]	0.092(14)	0.112(17)
0.10593	1.59375	[35, 47]	1.46(14)	1.79(17)	[36, 46]	0.113(20)	0.138(24)
0.096211	0	[32, 46]	1.359(72)	1.89(10)	[35, 48]	0.0089(57)	0.0124(79)
0.096211	0.1875	[34, 46]	1.380(72)	1.92(10)	[25, 43]	0.0268(85)	0.037(12)
0.096211	0.375	[32, 47]	1.350(74)	1.88(10)	[30, 46]	0.0381(66)	0.0530(92)
0.096211	0.65625	[33, 47]	1.352(77)	1.88(11)	[35, 48]	0.0580(74)	0.081(10)
0.096211	0.9375	[36, 47]	1.355(82)	1.88(11)	[28, 47]	0.0810(96)	0.112(13)
0.096211	1.3125	[36, 46]	1.37(10)	1.90(14)	[36, 48]	0.106(13)	0.147(18)
0.096211	1.59375	[35, 46]	1.39(13)	1.93(18)	[40, 47]	0.125(19)	0.174(26)

TABLE XVIII. h_{A_1} extracted on Ensemble F6.

κ_h	Range	$\langle D_s^* | \vec{A}^I | H_s \rangle_{\parallel}^R$	h_{A_1}	$\Sigma_{h_{A1}}$
0.12713	[9, 28]	1.22(10)	0.853(70)	$\cdots$
0.1237	[12, 28]	1.31(14)	0.872(94)	1.022(34)
0.119241	[17, 41]	1.36(19)	0.88(13)	1.010(56)
0.113382	[21, 42]	1.40(23)	0.89(15)	1.013(37)
0.10593	[24, 38]	1.44(23)	0.93(15)	1.04(24)
0.096211	[28, 40]	1.37(27)	0.92(18)	0.99(26)

TABLE XIX. $\mathcal{G}$ at zero recoil and $\Sigma_i = \frac{\mathcal{G}_i}{\mathcal{G}_{i-1}}$ on F6.

Scaling step	$\mathcal{G}(w=1)$	$\Sigma_{\mathcal{G}}$
D_s	0.966(50)	$\cdots$
1	0.959(58)	0.9929(10)
2	0.967(72)	1.0084(11)
3	0.984(86)	1.0177(13)
4	0.911(82)	0.9255(40)
5	1.104(98)	1.2121(55)

TABLE XX. Pseudoscalar masses on F7.

κ_h	Range	am_p
0.12713	[13, 37]	0.65511(28)
0.123649	[14, 32]	0.77744(47)
0.119196	[11, 35]	0.91865(36)
0.11335	[10, 29]	1.08532(41)
0.105786	[8, 25]	1.28215(44)
0.096689	[7, 23]	1.50077(43)

TABLE XXI. Improved and renormalized hadronic matrix elements $\langle D_s|V_\mu|H_s\rangle$ on F7.

κ_h	θ	Range	V_0^I	V_0^{IR}	Range	V_n^I	V_n^{IR}
0.12713	0	[8, 40]	1.272(26)	1.212(25)	[14, 45]	0.0031(16)	0.0030(15)
0.12713	0.1875	[8, 44]	1.254(44)	1.194(42)	[6, 45]	0.0094(29)	0.0089(27)
0.12713	0.375	[9, 43]	1.253(44)	1.194(42)	[24, 39]	0.0213(52)	0.0203(49)
0.12713	0.65625	[8, 43]	1.227(40)	1.169(38)	[23, 43]	0.0307(57)	0.0293(54)
0.12713	0.9375	[7, 41]	1.226(41)	1.168(39)	[18, 45]	0.0471(58)	0.0448(55)
0.12713	1.3125	[11, 43]	1.340(69)	1.276(65)	[9, 43]	0.0804(51)	0.0766(49)
0.12713	1.59375	[13, 45]	1.325(76)	1.262(72)	[12, 39]	0.0971(65)	0.0925(62)
0.123649	0	[13, 40]	1.307(31)	1.295(31)	[12, 45]	0.0035(17)	0.0034(16)
0.123649	0.1875	[5, 44]	1.286(51)	1.274(50)	[22, 43]	0.0117(41)	0.0116(41)
0.123649	0.375	[6, 42]	1.285(51)	1.273(50)	[26, 48]	0.0230(41)	0.0228(40)
0.123649	0.65625	[7, 44]	1.255(48)	1.244(47)	[17, 44]	0.0333(56)	0.0330(56)
0.123649	0.9375	[7, 39]	1.250(51)	1.239(50)	[20, 46]	0.0490(60)	0.0486(59)
0.123649	1.3125	[11, 41]	1.384(85)	1.371(84)	[11, 43]	0.0866(60)	0.0858(59)
0.123649	1.59375	[10, 44]	1.367(94)	1.355(93)	[12, 42]	0.1029(71)	0.1020(71)
0.119196	0	[14, 42]	1.339(33)	1.395(34)	[18, 45]	0.0039(20)	0.0040(21)
0.119196	0.1875	[12, 43]	1.313(55)	1.368(57)	[22, 44]	0.0121(43)	0.0126(45)
0.119196	0.375	[10, 42]	1.312(56)	1.367(58)	[25, 45]	0.0232(46)	0.0242(48)
0.119196	0.65625	[16, 46]	1.291(50)	1.345(52)	[20, 43]	0.0349(57)	0.0364(60)
0.119196	0.9375	[14, 44]	1.291(55)	1.345(57)	[20, 46]	0.0515(60)	0.0536(62)
0.119196	1.3125	[15, 43]	1.420(98)	1.48(10)	[11, 42]	0.0924(73)	0.0963(76)
0.119196	1.59375	[13, 43]	1.40(11)	1.46(11)	[10, 42]	0.1092(84)	0.1138(88)
0.11335	0	[21, 45]	1.305(30)	1.453(34)	[21, 38]	0.0033(34)	0.0037(38)
0.11335	0.1875	[21, 45]	1.349(47)	1.502(53)	[22, 43]	0.0140(55)	0.0156(61)
0.11335	0.375	[20, 44]	1.345(49)	1.498(54)	[23, 45]	0.0250(50)	0.0278(56)
0.11335	0.65625	[23, 45]	1.314(54)	1.463(61)	[24, 45]	0.0437(62)	0.0487(69)
0.11335	0.9375	[19, 44]	1.321(61)	1.470(68)	[21, 46]	0.0610(62)	0.0679(69)
0.11335	1.3125	[18, 44]	1.279(75)	1.424(83)	[16, 36]	0.0828(96)	0.092(11)
0.11335	1.59375	[21, 45]	1.268(81)	1.412(91)	[23, 43]	0.0860(96)	0.096(11)
0.105786	0	[26, 44]	1.294(30)	1.573(37)	[22, 41]	0.0044(37)	0.0053(45)
0.105786	0.1875	[30, 47]	1.328(44)	1.615(54)	[22, 43]	0.0144(58)	0.0175(71)
0.105786	0.375	[30, 46]	1.324(45)	1.609(55)	[24, 45]	0.0254(52)	0.0309(63)
0.105786	0.65625	[22, 45]	1.299(57)	1.579(69)	[25, 45]	0.0459(61)	0.0558(74)
0.105786	0.9375	[22, 45]	1.312(61)	1.596(74)	[23, 44]	0.0641(74)	0.0779(90)
0.105786	1.3125	[23, 45]	1.272(69)	1.546(84)	[19, 35]	0.079(12)	0.097(15)
0.105786	1.59375	[22, 46]	1.259(85)	1.53(10)	[22, 44]	0.085(10)	0.104(12)
0.096689	0	[28, 44]	1.310(30)	1.782(41)	[25, 39]	0.0098(43)	0.0133(58)
0.096689	0.1875	[24, 42]	1.261(65)	1.715(88)	[23, 42]	0.0240(60)	0.0327(82)
0.096689	0.375	[26, 45]	1.254(59)	1.705(80)	[22, 39]	0.0342(74)	0.046(10)
0.096689	0.65625	[27, 45]	1.333(60)	1.813(81)	[23, 38]	0.045(10)	0.061(14)
0.096689	0.9375	[25, 45]	1.353(64)	1.840(88)	[23, 41]	0.0611(87)	0.083(12)
0.096689	1.3125	[24, 39]	1.343(79)	1.83(11)	[24, 41]	0.104(11)	0.142(15)
0.096689	1.59375	[28, 46]	1.305(74)	1.78(10)	[22, 44]	0.113(12)	0.153(16)

TABLE XXII. h_{A_1} extracted on Ensemble F7.

κ_h	Range	$\langle D_s^*|\vec{A}^I|H_s\rangle_\parallel^R$	h_{A_1}	$\Sigma_{h_{A_1}}$
0.12713	[15, 25]	1.175(41)	0.825(29)	$\cdots$
0.123649	[14, 30]	1.211(52)	0.813(35)	0.985(15)
0.119196	[14, 34]	1.263(67)	0.820(43)	1.009(15)
0.11335	[16, 34]	1.226(83)	0.782(53)	0.954(80)
0.105786	[19, 33]	1.24(10)	0.794(65)	1.015(22)
0.096689	[22, 33]	1.16(14)	0.771(90)	0.97(13)

TABLE XXIII. $\mathcal{G}$ at zero recoil and $\Sigma_i = \frac{\mathcal{G}_i}{\mathcal{G}_{i-1}}$ on F7.

Scaling step	$\mathcal{G}(w = 1)$	$\Sigma_\mathcal{G}$
D_s	0.929(20)	$\cdots$
1	0.901(25)	0.9702(11)
2	0.882(30)	0.97820(88)
3	0.889(38)	1.0078(40)
4	0.908(48)	1.0214(10)
5	0.987(72)	1.0875(58)

TABLE XXIV.   Pseudoscalar masses on G8.

κ_h	Range	am_p
0.1271	[19, 45]	0.65660(86)
0.123719	[13, 39]	0.77676(98)
0.11926	[13, 32]	0.9179(11)
0.113447	[12, 33]	1.0843(12)
0.105836	[8, 26]	1.28537(91)
0.096143	[5, 24]	1.52492(90)

TABLE XXV.   Improved and renormalized hadronic matrix elements $\langle D_s|V_\mu|H_s\rangle$ on G8.

κ_h	θ	Range	V_0^I	V_0^{IR}	Range	V_n^I	V_n^{IR}
0.1271	0	[11, 53]	1.31(17)	1.25(16)	[21, 53]	0.0127(62)	0.0121(59)
0.1271	0.25	[9, 54]	1.28(15)	1.22(14)	[9, 51]	0.0242(98)	0.0230(93)
0.1271	0.5	[8, 55]	1.28(15)	1.22(14)	[14, 48]	0.034(13)	0.032(13)
0.1271	0.875	[11, 55]	1.26(15)	1.20(14)	[9, 48]	0.054(13)	0.051(12)
0.1271	1.25	[11, 54]	1.32(16)	1.26(15)	[17, 49]	0.070(16)	0.067(15)
0.1271	1.75	[9, 52]	1.33(16)	1.27(15)	[13, 48]	0.090(21)	0.086(20)
0.1271	2.125	[11, 55]	1.35(18)	1.28(17)	[12, 48]	0.104(23)	0.099(22)
0.123719	0	[18, 53]	1.36(21)	1.35(21)	[22, 56]	0.0129(66)	0.0128(65)
0.123719	0.25	[19, 57]	1.32(18)	1.30(18)	[22, 56]	0.022(12)	0.021(12)
0.123719	0.5	[16, 57]	1.32(18)	1.31(17)	[23, 55]	0.034(14)	0.034(14)
0.123719	0.875	[21, 57]	1.29(18)	1.28(17)	[21, 51]	0.058(16)	0.057(16)
0.123719	1.25	[23, 56]	1.36(18)	1.35(18)	[26, 43]	0.088(24)	0.087(24)
0.123719	1.75	[21, 56]	1.37(22)	1.36(22)	[27, 43]	0.122(31)	0.121(30)
0.123719	2.125	[22, 61]	1.38(27)	1.37(26)	[24, 52]	0.123(29)	0.122(29)
0.11926	0	[26, 56]	1.38(23)	1.44(24)	[29, 53]	0.0139(69)	0.0145(72)
0.11926	0.25	[26, 59]	1.33(23)	1.39(24)	[28, 57]	0.018(12)	0.019(13)
0.11926	0.5	[23, 54]	1.33(20)	1.39(21)	[28, 41]	0.053(29)	0.055(30)
0.11926	0.875	[24, 56]	1.29(20)	1.35(21)	[21, 39]	0.065(30)	0.068(31)
0.11926	1.25	[25, 59]	1.37(21)	1.43(22)	[26, 42]	0.098(32)	0.102(33)
0.11926	1.75	[26, 55]	1.39(26)	1.45(27)	[24, 43]	0.118(35)	0.123(37)
0.11926	2.125	[24, 52]	1.41(32)	1.47(34)	[29, 50]	0.142(38)	0.148(39)
0.113447	0	[31, 56]	1.44(25)	1.60(28)	[29, 44]	0.022(17)	0.025(19)
0.113447	0.25	[30, 55]	1.44(25)	1.60(28)	[29, 48]	0.029(23)	0.033(25)
0.113447	0.5	[30, 58]	1.43(22)	1.60(24)	[28, 42]	0.054(33)	0.061(37)
0.113447	0.875	[34, 62]	1.38(21)	1.54(23)	[31, 50]	0.061(24)	0.068(27)
0.113447	1.25	[31, 54]	1.39(22)	1.55(25)	[29, 46]	0.088(32)	0.098(35)
0.113447	1.75	[33, 57]	1.40(27)	1.56(30)	[29, 44]	0.121(43)	0.135(48)
0.113447	2.125	[37, 61]	1.41(33)	1.57(36)	[27, 42]	0.161(61)	0.179(68)
0.105836	0	[37, 54]	1.47(27)	1.79(32)	[37, 55]	0.0161(84)	0.020(10)
0.105836	0.25	[40, 62]	1.41(22)	1.72(26)	[35, 51]	0.028(21)	0.034(26)
0.105836	0.5	[35, 55]	1.47(23)	1.79(28)	[33, 46]	0.043(33)	0.052(41)
0.105836	0.875	[36, 57]	1.41(22)	1.72(27)	[38, 59]	0.035(20)	0.042(25)
0.105836	1.25	[36, 56]	1.41(22)	1.72(27)	[34, 45]	0.084(44)	0.102(53)
0.105836	1.75	[40, 60]	1.40(25)	1.70(31)	[35, 47]	0.111(52)	0.136(63)
0.105836	2.125	[39, 59]	1.46(35)	1.78(43)	[38, 57]	0.091(46)	0.111(56)
0.096143	0	[39, 56]	1.49(27)	2.05(37)	[35, 49]	0.028(20)	0.038(28)
0.096143	0.25	[38, 51]	1.56(32)	2.14(43)	[38, 51]	0.035(32)	0.048(44)
0.096143	0.5	[38, 53]	1.54(29)	2.12(40)	[38, 49]	0.050(36)	0.068(49)
0.096143	0.875	[38, 56]	1.46(25)	2.00(34)	[40, 54]	0.047(35)	0.064(49)
0.096143	1.25	[39, 52]	1.50(28)	2.06(38)	[40, 51]	0.084(47)	0.115(64)
0.096143	1.75	[39, 53]	1.51(34)	2.08(46)	[39, 49]	0.123(70)	0.169(96)
0.096143	2.125	[43, 62]	1.44(34)	1.98(46)	[39, 51]	0.123(78)	0.17(11)

TABLE XXVI. $\mathcal{G}$ at zero recoil and $\Sigma_i = \frac{\mathcal{G}_i}{\mathcal{G}_{i-1}}$ on G8.

Scaling step	$\mathcal{G}(w=1)$	$\Sigma_{\mathcal{G}}$
D_s	0.92(11)	...
1	0.95(16)	1.02726(97)
2	0.98(24)	1.0322(13)
3	1.04(20)	1.0640(15)
4	0.96(21)	0.9256(17)
5	1.16(40)	1.2036(32)

TABLE XXVII. Pseudoscalar masses on N6.

κ_h	Range	am_p
0.13026	[17, 40]	0.48394(56)
0.127737	[16, 38]	0.58010(66)
0.124958	[13, 37]	0.67722(66)
0.121051	[15, 35]	0.79993(87)
0.115915	[15, 29]	0.9483(10)
0.109399	[10, 23]	1.12221(93)

TABLE XXVIII. Improved and renormalized hadronic matrix elements $\langle D_s|V_\mu|H_s\rangle$ on N6.

κ_h	θ	Range	V_0^I	V_0^{IR}	Range	V_n^I	V_n^{IR}
0.13026	0	[5, 44]	1.019(38)	0.931(35)	[13, 46]	0.0051(24)	0.0047(22)
0.13026	0.2535	[17, 42]	1.038(39)	0.947(36)	[19, 45]	0.0221(34)	0.0202(31)
0.13026	0.507	[23, 45]	1.046(41)	0.955(38)	[22, 46]	0.0390(39)	0.0356(36)
0.13026	0.887	[16, 44]	1.061(47)	0.969(43)	[15, 43]	0.0632(53)	0.0577(49)
0.13026	1.2675	[23, 45]	1.110(59)	1.013(54)	[16, 45]	0.0895(67)	0.0817(61)
0.13026	1.774	[27, 48]	1.221(71)	1.115(65)	[14, 45]	0.1343(78)	0.1226(71)
0.13026	2.1545	[31, 47]	1.30(12)	1.19(11)	[21, 44]	0.161(15)	0.147(14)
0.127737	0	[12, 45]	1.080(43)	1.016(41)	[12, 46]	0.0048(25)	0.0046(23)
0.127737	0.2535	[12, 42]	1.101(46)	1.036(43)	[17, 44]	0.0230(35)	0.0216(33)
0.127737	0.507	[23, 46]	1.104(47)	1.039(44)	[16, 42]	0.0412(45)	0.0388(42)
0.127737	0.887	[23, 46]	1.118(55)	1.052(52)	[15, 43]	0.0670(58)	0.0631(54)
0.127737	1.2675	[14, 45]	1.178(63)	1.108(59)	[16, 44]	0.0945(75)	0.0889(70)
0.127737	1.774	[24, 47]	1.290(76)	1.214(71)	[12, 46]	0.1417(84)	0.1334(79)
0.127737	2.1545	[32, 47]	1.40(13)	1.32(13)	[19, 45]	0.173(15)	0.163(14)
0.124958	0	[18, 45]	1.126(44)	1.095(43)	[12, 48]	0.0047(25)	0.0045(25)
0.124958	0.2535	[26, 46]	1.139(46)	1.108(44)	[17, 44]	0.0237(37)	0.0230(36)
0.124958	0.507	[28, 46]	1.143(48)	1.111(47)	[16, 45]	0.0427(42)	0.0415(41)
0.124958	0.887	[30, 45]	1.155(58)	1.123(57)	[16, 44]	0.0697(60)	0.0678(59)
0.124958	1.2675	[28, 47]	1.218(74)	1.184(72)	[15, 43]	0.0991(82)	0.0964(80)
0.124958	1.774	[15, 46]	1.347(74)	1.310(72)	[13, 43]	0.1477(98)	0.1436(95)
0.124958	2.1545	[29, 47]	1.46(13)	1.42(13)	[19, 44]	0.180(17)	0.175(16)
0.121051	0	[25, 47]	1.148(46)	1.169(47)	[12, 46]	0.0043(28)	0.0044(29)
0.121051	0.2535	[29, 46]	1.171(49)	1.192(50)	[16, 44]	0.0242(38)	0.0246(39)
0.121051	0.507	[23, 46]	1.185(54)	1.206(55)	[15, 44]	0.0440(46)	0.0447(47)
0.121051	0.887	[28, 46]	1.194(64)	1.215(65)	[17, 44]	0.0717(65)	0.0730(67)
0.121051	1.2675	[27, 46]	1.262(80)	1.285(81)	[15, 43]	0.1015(92)	0.1033(93)
0.121051	1.774	[17, 46]	1.401(87)	1.426(88)	[12, 43]	0.151(11)	0.154(12)
0.121051	2.1545	[22, 47]	1.49(12)	1.52(13)	[20, 44]	0.184(19)	0.188(20)
0.115915	0	[37, 47]	1.149(43)	1.241(46)	[11, 42]	0.0051(28)	0.0055(30)
0.115915	0.2535	[31, 46]	1.190(50)	1.285(54)	[18, 43]	0.0247(43)	0.0266(46)
0.115915	0.507	[26, 45]	1.208(56)	1.304(61)	[16, 41]	0.0458(57)	0.0494(61)
0.115915	0.887	[27, 46]	1.221(67)	1.319(73)	[16, 44]	0.0738(70)	0.0797(76)
0.115915	1.2675	[31, 47]	1.283(83)	1.386(90)	[14, 45]	0.1044(98)	0.113(11)
0.115915	1.774	[22, 46]	1.453(97)	1.57(10)	[21, 42]	0.147(15)	0.159(16)
0.115915	2.1545	[24, 47]	1.55(14)	1.67(15)	[19, 45]	0.194(21)	0.210(23)
0.109399	0	[33, 45]	1.164(42)	1.357(49)	[14, 36]	0.0093(38)	0.0108(44)
0.109399	0.2535	[32, 46]	1.192(46)	1.389(54)	[30, 47]	0.0254(38)	0.0296(44)
0.109399	0.507	[35, 47]	1.186(49)	1.382(57)	[26, 44]	0.0467(51)	0.0544(59)
0.109399	0.887	[36, 47]	1.198(61)	1.396(71)	[26, 45]	0.0763(71)	0.0889(82)
0.109399	1.2675	[37, 47]	1.269(80)	1.478(93)	[22, 45]	0.106(11)	0.123(12)
0.109399	1.774	[25, 47]	1.481(100)	1.73(12)	[23, 43]	0.150(16)	0.175(19)
0.109399	2.1545	[27, 47]	1.59(15)	1.85(18)	[31, 45]	0.215(29)	0.250(34)

TABLE XXIX. h_{A_1} extracted on Ensemble N6.

κ_h	Range	$\langle D_s^* \vert \vec{A}^I \vert H_s \rangle_{\parallel}^R$	h_{A_1}	$\Sigma_{h_{A1}}$
0.13026	[14, 39]	0.818(65)	0.741(58)	$\cdots$
0.127737	[27, 43]	0.865(97)	0.738(82)	0.996(46)
0.124958	[26, 43]	0.90(10)	0.736(84)	0.9971(97)
0.121051	[15, 39]	0.93(10)	0.732(81)	0.994(31)
0.115915	[20, 42]	0.97(12)	0.739(91)	1.011(23)
0.109399	[25, 43]	1.01(13)	0.765(97)	1.034(24)

TABLE XXX. $\mathcal{G}$ at zero recoil and $\Sigma_i = \frac{\mathcal{G}_i}{\mathcal{G}_{i-1}}$ on N6.

Scaling step	$\mathcal{G}(w = 1)$	$\Sigma_{\mathcal{G}}$
D_s	0.962(40)	$\cdots$
1	0.969(44)	1.00785(86)
2	0.967(46)	0.99763(67)
3	0.968(54)	1.00106(84)
4	0.968(64)	0.9996(11)
5	0.967(62)	0.9990(17)

TABLE XXXI. Pseudoscalar masses on O7.

κ_h	Range	am_p
0.13022	[15, 44]	0.48290(95)
0.1279	[17, 42]	0.5707(10)
0.124944	[17, 44]	0.6729(12)
0.12091	[16, 41]	0.7990(13)
0.11589	[13, 34]	0.9433(12)
0.1094	[8, 28]	1.1156(13)

TABLE XXXII. Improved and renormalized hadronic matrix elements $\langle D_s \vert V_\mu \vert H_s \rangle$ on O7.

κ_h	θ	Range	V_0^I	V_0^{IR}	Range	V_n^I	V_n^{IR}
0.13022	0	[15, 59]	0.95(11)	0.871(98)	[13, 62]	0.0071(36)	0.0065(33)
0.13022	0.338	[18, 60]	0.944(80)	0.863(73)	[35, 63]	0.0211(64)	0.0193(59)
0.13022	0.676	[9, 59]	0.885(82)	0.809(75)	[36, 58]	0.022(11)	0.0205(96)
0.13022	1.183	[42, 61]	0.848(92)	0.776(84)	[26, 62]	0.049(11)	0.0446(97)
0.13022	1.683	[43, 61]	0.79(14)	0.72(13)	[34, 64]	0.061(14)	0.056(13)
0.13022	2.365	[34, 62]	0.79(20)	0.72(18)	[49, 64]	0.096(37)	0.088(34)
0.13022	2.873	[28, 63]	0.82(26)	0.75(24)	[38, 62]	0.061(38)	0.056(34)
0.1279	0	[12, 61]	0.98(12)	0.92(11)	[30, 59]	0.0089(46)	0.0084(43)
0.1279	0.338	[36, 59]	0.986(84)	0.927(79)	[38, 62]	0.0214(72)	0.0201(68)
0.1279	0.676	[18, 60]	0.935(88)	0.879(83)	[38, 61]	0.0334(83)	0.0314(78)
0.1279	1.183	[37, 61]	0.881(97)	0.828(91)	[32, 61]	0.051(11)	0.048(10)
0.1279	1.683	[40, 62]	0.82(15)	0.77(14)	[28, 60]	0.061(15)	0.057(14)
0.1279	2.365	[38, 60]	0.81(23)	0.76(22)	[37, 60]	0.065(31)	0.061(29)
0.1279	2.873	[38, 62]	0.93(44)	0.87(42)	[34, 60]	0.067(33)	0.063(31)
0.124944	0	[22, 60]	1.02(13)	0.99(13)	[26, 59]	0.0086(48)	0.0084(47)
0.124944	0.338	[36, 61]	1.021(90)	0.994(88)	[39, 61]	0.0214(82)	0.0208(80)
0.124944	0.676	[30, 61]	0.969(95)	0.943(93)	[36, 59]	0.0335(94)	0.0326(92)
0.124944	1.183	[31, 63]	0.91(10)	0.88(10)	[30, 60]	0.052(12)	0.051(12)
0.124944	1.683	[32, 61]	0.84(15)	0.82(14)	[31, 62]	0.066(16)	0.064(15)
0.124944	2.365	[32, 61]	0.81(24)	0.79(23)	[46, 64]	0.094(41)	0.092(40)
0.124944	2.873	[20, 62]	0.78(30)	0.76(29)	[35, 62]	0.064(48)	0.062(47)
0.12091	0	[37, 63]	1.05(13)	1.07(13)	[32, 58]	0.0075(53)	0.0076(54)
0.12091	0.338	[44, 61]	1.055(93)	1.076(95)	[39, 61]	0.0214(91)	0.0218(93)
0.12091	0.676	[40, 61]	0.95(14)	0.97(14)	[28, 59]	0.032(10)	0.033(10)
0.12091	1.183	[34, 62]	0.94(15)	0.96(15)	[33, 59]	0.054(13)	0.055(13)
0.12091	1.683	[29, 61]	0.86(17)	0.87(17)	[33, 62]	0.069(16)	0.070(17)
0.12091	2.365	[29, 61]	0.80(29)	0.81(30)	[35, 62]	0.075(28)	0.076(29)
0.12091	2.873	[24, 62]	0.75(43)	0.76(44)	[47, 61]	0.121(98)	0.123(100)

(Table continued)

TABLE XXXII. *(Continued)*

κ_h	θ	Range	V_0^I	V_0^{IR}	Range	V_n^I	V_n^{IR}
0.11589	0	[42, 61]	1.07(13)	1.16(14)	[32, 61]	0.0070(45)	0.0076(49)
0.11589	0.338	[43, 61]	1.068(95)	1.15(10)	[39, 59]	0.019(11)	0.020(12)
0.11589	0.676	[49, 63]	1.00(13)	1.08(15)	[40, 61]	0.0304(96)	0.033(10)
0.11589	1.183	[40, 62]	0.95(15)	1.03(16)	[33, 62]	0.057(13)	0.062(14)
0.11589	1.683	[32, 62]	0.86(17)	0.93(19)	[32, 61]	0.070(18)	0.075(19)
0.11589	2.365	[30, 60]	0.79(33)	0.85(36)	[46, 63]	0.100(45)	0.108(49)
0.11589	2.873	[30, 61]	0.81(56)	0.87(60)	[42, 64]	0.114(85)	0.123(92)
0.1094	0	[41, 61]	1.09(13)	1.27(16)	[38, 60]	0.0124(58)	0.0145(68)
0.1094	0.338	[38, 61]	1.04(13)	1.21(16)	[45, 61]	0.0190(100)	0.022(12)
0.1094	0.676	[39, 61]	0.96(15)	1.12(17)	[46, 62]	0.034(18)	0.040(21)
0.1094	1.183	[37, 62]	0.93(12)	1.08(14)	[37, 60]	0.054(14)	0.063(17)
0.1094	1.683	[36, 63]	0.84(19)	0.98(22)	[36, 61]	0.073(16)	0.085(19)
0.1094	2.365	[36, 62]	0.90(57)	1.05(66)	[44, 61]	0.19(11)	0.22(12)
0.1094	2.873	[35, 61]	0.55(70)	0.65(82)	[42, 62]	0.086(59)	0.100(69)

TABLE XXXIII. h_{A_1} extracted on Ensemble O7.

κ_h	Range	$\langle D_s^* \vert \vec{A}^I \vert H_s \rangle_{\parallel}^R$	h_{A_1}	$\Sigma_{h_{A1}}$
0.13022	[8, 31]	0.74(12)	0.68(11)	$\cdots$
0.1279	[7, 30]	0.75(15)	0.65(13)	0.949(57)
0.124944	[33, 47]	0.90(24)	0.74(20)	1.15(16)
0.12091	[28, 49]	1.08(28)	0.86(22)	1.15(16)
0.11589	[28, 48]	1.15(32)	0.89(25)	1.039(48)
0.1094	[33, 46]	2.06(66)	1.58(51)	1.77(88)

TABLE XXXIV. $\mathcal{G}$ at zero recoil and $\Sigma_i = \frac{\mathcal{G}_i}{\mathcal{G}_{i-1}}$ on O7.

Scaling step	$\mathcal{G}(w=1)$	$\Sigma_{\mathcal{G}}$
D_s	0.859(70)	$\cdots$
1	0.861(76)	1.00251(33)
2	0.846(84)	0.98217(34)
3	0.826(91)	0.97726(68)
4	0.80(10)	0.96533(41)
5	0.79(13)	0.98804(97)

[1] J. Lees *et al.* (*BABAR* Collaboration), Evidence for an Excess of $\bar{B} \to D^{(*)}\tau^-\bar{\nu}_\tau$ Decays, Phys. Rev. Lett. **109,** 101802 (2012).

[2] J. Lees *et al.* (*BABAR* Collaboration), Measurement of an excess of $\bar{B} \to D^{(*)}\tau^-\bar{\nu}_\tau$ decays and implications for charged Higgs bosons, Phys. Rev. D **88,** 072012 (2013).

[3] M. Huschle *et al.* (Belle Collaboration), Measurement of the branching ratio of $\bar{B} \to D^{(*)}\tau^-\bar{\nu}_\tau$ relative to $\bar{B} \to D^{(*)}\ell^-\bar{\nu}_\ell$ decays with hadronic tagging at Belle, Phys. Rev. D **92,** 072014 (2015).

[4] R. Aaij *et al.* (LHCb Collaboration), Measurement of the Ratio of Branching Fractions $\mathcal{B}(\bar{B}^0 \to D^{*+}\tau^-\bar{\nu}_\tau)/\mathcal{B}(\bar{B}^0 \to D^{*+}\mu^-\bar{\nu}_\mu)$, Phys. Rev. Lett. **115,** 111803 (2015); **115,** 159901(E) (2015).

[5] Y. Sato *et al.* (Belle Collaboration), Measurement of the branching ratio of $\bar{B}^0 \to D^{*+}\tau^-\bar{\nu}_\tau$ relative to $\bar{B}^0 \to D^{*+}\ell^-\bar{\nu}_\ell$ decays with a semileptonic tagging method, Phys. Rev. D **94,** 072007 (2016).

[6] J. A. Bailey *et al.* (MILC Collaboration), $B \to D\ell\nu$ form factors at nonzero recoil and $|V_{cb}|$ from 2 + 1-flavor lattice QCD, Phys. Rev. D **92,** 034506 (2015).

[7] H. Na, C. M. Bouchard, G. P. Lepage, C. Monahan, and J. Shigemitsu (HPQCD Collaboration), $B \to Dl\nu$ form factors at nonzero recoil and extraction of $|V_{cb}|$, Phys. Rev. D **92,** 054510 (2015); **93,** 119906(E) (2016).

[8] D. Bigi and P. Gambino, Revisiting $B \to D\ell\nu$, Phys. Rev. D **94,** 094008 (2016).

[9] F. U. Bernlochner, Z. Ligeti, M. Papucci, and D. J. Robinson, Combined analysis of semileptonic B decays to D and D^*: $R(D^{(*)})$, $|V_{cb}|$, and new physics, Phys. Rev. D **95,** 115008 (2017); **97,** 059902(E) (2018).

[10] S. Jaiswal, S. Nandi, and S. K. Patra, Extraction of $|V_{cb}|$ from $B \to D^{(*)}\ell\nu_\ell$ and the Standard Model predictions of $R(D^{(*)})$, J. High Energy Phys. 12 (2017) 060.

[11] S. Hirose *et al.* (Belle Collaboration), Measurement of the τ Lepton Polarization and $R(D^*)$ in the Decay $\bar{B} \to D^*\tau^-\bar{\nu}_\tau$, Phys. Rev. Lett. **118,** 211801 (2017).

[12] S. Hirose *et al.* (Belle Collaboration), Measurement of the τ lepton polarization and $R(D^*)$ in the decay $\bar{B} \to D^*\tau^-\bar{\nu}_\tau$ with one-prong hadronic τ decays at Belle, Phys. Rev. D **97,** 012004 (2018).

[13] R. Aaij *et al.* (LHCb Collaboration), Measurement of the Ratio of the $B^0 \to D^{*-}\tau^+\nu_\tau$ and $B^0 \to D^{*-}\mu^+\nu_\mu$ Branching Fractions using Three-Prong τ-Lepton Decays, Phys. Rev. Lett. **120,** 171802 (2018).

[14] R. Aaij *et al.* (LHCb Collaboration), Test of lepton flavor universality by the measurement of the $B^0 \to D^{*-}\tau^+\nu_\tau$ branching fraction using three-prong τ decays, Phys. Rev. D **97,** 072013 (2018).

[15] D. Bigi, P. Gambino, and S. Schacht, $R(D^*)$, $|V_{cb}|$, and the heavy quark symmetry relations between form factors, J. High Energy Phys. 11 (2017) 061.

[16] R. Aaij *et al.* (LHCb Collaboration), Measurement of the Ratio of Branching Fractions $\mathcal{B}(B_c^+ \to J/\psi\tau^+\nu_\tau)/\mathcal{B}(B_c^+ \to J/\psi\mu^+\nu_\mu)$, Phys. Rev. Lett. **120,** 121801 (2018).

[17] J. Harrison, C. T. H. Davies, and A. Lytle (HPQCD Collaboration), $R(J/\psi)$ and $B_c^- \to J/\psi\ell^-\bar{\nu}_l$ Lepton Flavor Universality Violating Observables from Lattice QCD, Phys. Rev. Lett. **125,** 222003 (2020).

[18] S. Fajfer, J. F. Kamenik, and I. Nisandzic, On the $B \to D^*\tau\bar{\nu}_\tau$ Sensitivity to new physics, Phys. Rev. D **85,** 094025 (2012).

[19] L. Di Luzio, A. Greljo, and M. Nardecchia, Gauge leptoquark as the origin of B-physics anomalies, Phys. Rev. D **96,** 115011 (2017).

[20] M. Atoui, D. Becirevic, V. Morénas, and F. Sanfilippo, $B_s \to D_s\ell\nu_\ell$ near zero recoil in and beyond the Standard Model, arXiv:1310.5238v3.

[21] C. J. Monahan, H. Na, C. M. Bouchard, G. P. Lepage, and J. Shigemitsu, $B_s \to D_s\ell\nu$ form factors and the fragmentation fraction ratio f_s/f_d, Phys. Rev. D **95,** 114506 (2017).

[22] J. Harrison, C. Davies, and M. Wingate (HPQCD Collaboration), Lattice QCD calculation of the $B_{(s)} \to D^*_{(s)}\ell\nu$ form factors at zero recoil and implications for $|V_{cb}|$, Phys. Rev. D **97,** 054502 (2018).

[23] E. McLean, C. T. H. Davies, A. T. Lytle, and J. Koponen (HPQCD Collaboration), Lattice QCD form factor for $B_s \to D_s^*l\nu$ at zero recoil with non-perturbative current renormalisation, Phys. Rev. D **99,** 114512 (2019).

[24] E. McLean, C. T. H. Davies, J. Koponen, and A. T. Lytle (HPQCD Collaboration), $B_s \to D_s\ell\nu$ Form Factors for the full q^2 range from lattice QCD with non-perturbatively normalized currents, Phys. Rev. D **101,** 074513 (2020).

[25] J. Harrison and C. T. H. Davies (HPQCD Collaboration), $B_s \to D_s^*$ form factors for the full q^2 range from lattice QCD, arXiv:2105.11433.

[26] B. Blossier *et al.* (ETM Collaboration), A proposal for B-physics on current lattices, J. High Energy Phys. 04 (2010) 049.

[27] R. Balasubramamian and B. Blossier, Decay constant of B_s and B_s^* mesons from $N_f = 2$ lattice QCD, Eur. Phys. J. C **80,** 412 (2020).

[28] B. Sheikholeslami and R. Wohlert, Improved continuum limit lattice action for QCD with Wilson fermions, Nucl. Phys. **B259,** 572 (1985).

[29] M. Lüscher, S. Sint, R. Sommer, P. Weisz, and U. Wolff (ALPHA Collaboration), Nonperturbative O(a) improvement of lattice QCD, Nucl. Phys. **B491,** 323 (1997).

[30] K. G. Wilson, Confinement of quarks, Phys. Rev. D **10,** 2445 (1974).

[31] P. Fritzsch, F. Knechtli, B. Leder, M. Marinkovic, S. Schaefer, R. Sommer, and F. Virotta (ALPHA Collaboration), The strange quark mass and lambda parameter of two flavor QCD, Nucl. Phys. **B865,** 397 (2012).

[32] J. Heitger, G. M. von Hippel, S. Schaefer, and F. Virotta (ALPHA Collaboration), Charm quark mass and D-meson decay constants from two-flavour lattice QCD, Proc. Sci. LATTICE2013 (**2014**) 475.

[33] B. Blossier, J. Heitger, and M. Post, Leptonic D_s decays in two-flavor lattice QCD, Phys. Rev. D **98,** 054506 (2018).

[34] S. Lottini (ALPHA Collaboration), Chiral behaviour of the pion decay constant in $N_f = 2$ QCD, Proc. Sci. LATTICE2013 (**2014**) 315.

[35] U. Wolff (ALPHA Collaboration), Monte Carlo errors with less errors, Comput. Phys. Commun. **156,** 143 (2004). **176,** 383(E) (2007).

[36] M. Dalla Brida, T. Korzec, S. Sint, and P. Vilaseca, High precision renormalization of the flavour non-singlet Noether currents in lattice QCD with Wilson quarks, Eur. Phys. J. C **79,** 23 (2019).

[37] S. Sint and P. Weisz (ALPHA Collaboration), Further results on O(a) improved lattice QCD to one loop order of perturbation theory, Nucl. Phys. **B502,** 251 (1997).

[38] M. Guagnelli, R. Petronzio, J. Rolf, S. Sint, R. Sommer, and U. Wolff (ALPHA Collaboration), Nonperturbative results for the coefficients b_m and $b_A - b_P$ in O(a) improved lattice QCD, Nucl. Phys. **B595,** 44 (2001).

[39] J. A. Bailey *et al.* (Fermilab Lattice, MILC Collaborations), Update of $|V_{cb}|$ from the $\bar{B} \to D^*\ell\bar{\nu}$ form factor at zero recoil with three-flavor lattice QCD, Phys. Rev. D **89,** 114504 (2014).

[40] A. V. Avilés-Casco, C. DeTar, D. Du, A. El-Khadra, A. Kronfeld, J. Laiho, R. S. Van de Water, M. Della Morte, P. Fritzsch, E. Gámiz Sánchez, and C. Pena Ruano, $\bar{B} \to D^*\ell\bar{\nu}$ at Non-Zero Recoil, EPJ Web Conf. **175,** 13003 (2018).

[41] A. V. Avilés-Casco, C. DeTar, A. X. El-Khadra, A. S. Kronfeld, J. Laiho, and R. S. Van de Water (Fermilab Lattice, MILC Collaborations), The $B \to D^*\ell\nu$ semileptonic decay at nonzero recoil and its implications for $|V_{cb}|$ and $R(D^*)$, Proc. Sci., LATTICE2019 (**2019**) 049, arXiv:1912.05886].

[42] M. Bruno, D. Djukanovic, G. P. Engel, A. Francis, G. Herdoiza, H. Horch *et al.*, Simulation of QCD with $N_f = 2 + 1$ flavors of non-perturbatively improved Wilson fermions, J. High Energy Phys. 02 (2015) 043.

[43] G. S. Bali, E. E. Scholz, J. Simeth, and W. Söldner, Lattice simulations with $N_f = 2 + 1$ improved Wilson fermions at a fixed strange quark mass, Phys. Rev. D **94,** 074501 (2016).

[44] D. Mohler, S. Schaefer, and J. Simeth, CLS $2 + 1$ flavor simulations at physical light- and strange-quark masses, EPJ Web Conf. **175,** 02010 (2018).

[45] A. Francis, P. Fritzsch, M. Lüscher, and A. Rago, Master-field simulations of O(a)-improved lattice QCD: Algorithms, stability and exactness, Comput. Phys. Commun. **255,** 107355 (2020).

[46] F. Cuteri, A. Francis, P. Fritzsch, G. Pederiva, A. Rago, A. Shindler *et al.*, Properties, ensembles and hadron spectra with Stabilised Wilson Fermions (to be published).